CARBOXYMETHYLATION OF DEXTRAN FOR SURFACE MODIFICATION OF MAGNETITE NANOPARTICLES

by

Vanessa Ayala Rivera

A thesis submitted in partial fulfillment of the requirements for the degree of

MASTER OF SCIENCE
in
CHEMICAL ENGINEERING

UNIVERSITY OF PUERTO RICO
MAYAGÜEZ CAMPUS
2009

Approved by:

_____	_____
Madeline Torres-Lugo, PhD President, Graduate Committee	Date
_____	_____ Date
Carlos Rinaldi, PhD Member, Graduate Committee	
_____	_____
Franklin Carrero Martínez, PhD Member, Graduate Committee	Date
_____	_____
Gustavo Lopez, phD Representative of Graduate Studies	Date
_____	_____
David Suleiman, PhD Chairperson of the Department	Date

ABSTRACT

Magnetite nanoparticles are currently studied for biomedical applications such as MRI, drug delivery, and magnetic fluid hyperthermia (MHF). These applications require nanoparticles with a suitable coating which provides colloidal stability and improves the nanoparticle's transport and interaction with biological tissues. Polysaccharides such as dextran have been used for this purpose due to their biocompatibility, low toxicity, and versatility for nanoparticle suspension in cell culture media. Functionalization of magnetite nanoparticles with dextran was performed by carbodiimide chemistry in which amine groups previously grafted onto the nanoparticle's surface are reacted with carboxylic groups (-COOH) present in the dextran chain. These –COOH groups were introduced in the dextran chains by a carboxymethylation reaction, obtaining a carboxymethyl-dextran molecule (CMDx). The amount of –COOH groups per chain was controlled by different parameters such as reaction time, temperature, and sodium hydroxide and monochloroacetic acid ($ClCH_2COOH$) concentrations. CMDx with different degrees of substitution were prepared and the nanoparticle's surface charge and stability were studied using zeta potential measurements and dynamic light scattering. Results showed that decreasing the number of –COOH groups per dextran chain decrease the nanoparticle's surface charge without affecting their colloidal stability. The nanoparticles coated with CMDx with 5, 23 and 38 –COOH groups per dextran chain were stable over the entire range of pH and NaCl concentration studied.

ACKNOWLEDGEMENTS

During the development of my graduate studies in the University of Puerto Rico at Mayagüez several persons collaborated in one way or another with my research. Without their support it would be impossible for me to finish this work.

Firstly, I wish to thank my advisors, Dr. Madeline Torres-Lugo and Dr. Carlos Rinaldi for the opportunity they gave me to work under their guidance and supervision.

I want to acknowledge Adriana Herrera for her collaboration in this work, specially in the synthesis of the nanoparticles. I also want to sincerely thank her for the help, advise, and support she gave me during this process.

The NSF NIRT award 0609117 provided the funding and the resources for the development of this research.

Thanks to my family, for their unconditional love and support. A special mention to my mother for all the help and motivation she gave me and for being a mom of prayer.

At last, but the most important I would like to thank God for all the blessings He gave me and for giving me the opportunity to achieve this goal.

Table of Content

Table List

Figure List

1 INTRODUCTION

1.1 Nanotechnology

In his 1959 talk "There's Plenty of Room at the Bottom," Nobel prize physicist Richard Feynman was the first to suggest that materials could someday be fabricated with atomic specifications [1]. Research in what later became molecular manufacturing, resulted in the introduction of the term nanotechnology three decades after Feynman's talk. The term became popular and is now used to refer to technology which encompasses materials at the nanometer scale (1nm = 10^{-9} m = 10 Å), which have novel properties, and can be manipulated and controlled in a useful way.

Nanoparticles are essential components in nanotechnology because their specific properties are realized at the nanoparticle, nanocrystal, or nanolayer level. New physical (e.g., larger surface area), chemical, or biological properties as well as new phenomena (e.g., magnetic properties) are caused by size reduction [2]. Properties such as superparamagnetism are of increasing interest due to it's technological applications in a variety of fields including biomedicine [3].

1.2 Biomedical applications of nanoparticles

With the advent of nanotechnology in the last decade, it has become possible to synthesize, characterize, and especially modify the surface of nanoparticles for biomedical applications. Due to their promising properties, several investigations have been carried out in the biomedical field using nano scaled iron oxide particles, such as

magnetite (Fe_3O_4), for applications in magnetic bioseparations [4], drug delivery [5,6], MRI contrast agents [7,8], and treatment of cancer by hyperthermia [9, 10].

Currently, hyperthermia is achieved using different types of energy to apply heat, such as microwave, radiofrequency, ultrasound, thermal chambers, or hot water blankets (whole body hyperthermia), being almost always used in conjuction with other forms of cancer therapy [11]. This treatment takes advantage of the fact that cancer cells are more sensitive to heat than healthy cells [12]. At a temperature below 44 °C, most normal tissues will not be damaged, however, due to regional differences in tissue characteristics, some spots may achieve higher temperatures resulting in burns, blisters, discomfort, or pain [11]. In addition traditional cancer treatments, such as surgery, chemotherapy, and radiotherapy, also possess undesirable side effects or are highly invasive. For these reasons and taking advantage of the aforementioned properties, nanoparticles have gained attention in the search of alternative treatments and improvement of current techniques for cancer treatment. For hyperthermia, the challenge is the optimization of thermal homogeneity at the desired temperature.

The superparamagnetic properties of magnetite nanoparticles play an important role in the application of hyperthermia because this technique is based on magnetic losses due to relaxation losses and frictional losses. These losses are dissipated in the form of heat, resulting in an increase in the temperature of the surroundings [13]. The objective is to destroy the cancerous cells by increasing the temperature of the abnormal cells in a localized area when a magnetic field is applied, due to heat release. Magnetic fluid hyperthermia is achieved at a temperature range of 41° C to 46° C [9]. The main

advantage of using magnetic nanoparticles is that more homogeneous heating may be achieved [14]. Figure 1 shows a schematic representation of this approach.

For a material to be used in such applications it must meet certain criteria such as biocompatibility. According to Williams' definition [15], "*Biocompatibility refers to the ability of a material to perform with an appropriate host response in a specific situation.*"

Also biocompatibility refers to the quality of not having toxic or damaging effects on biological systems [16]. In other words, when in contact with a biological environment a biocompatible material should not cause harmful reactions or change its properties in an undesirable way. In addition to biocompatibility, size distribution, coating, and surface charge are crucial factors to be considered, and they will be addressed in the following chapter.

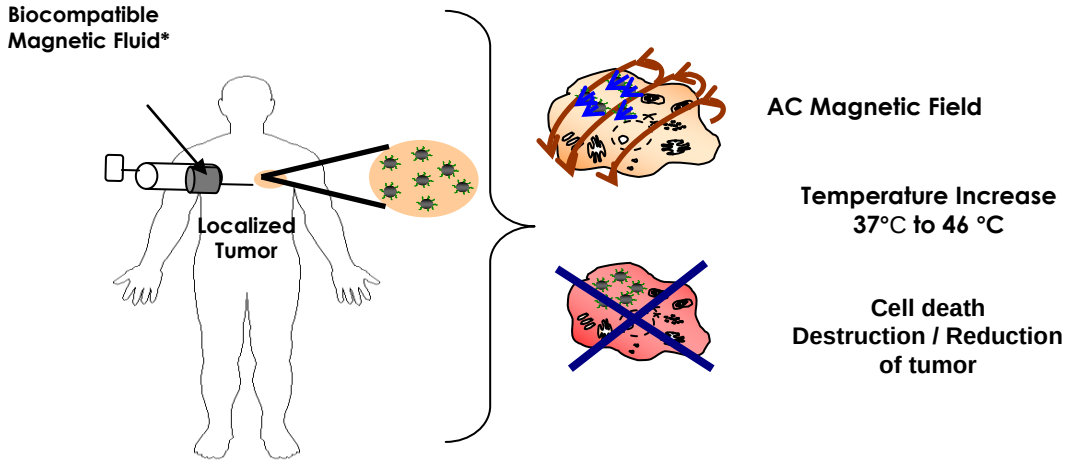

Figure 1. Magnetic Fluid Hyperthermia (MHF) process.

2 LITERATURE REVIEW

As we will see in this chapter, studies have shown that biodistribution strongly depends on the size, surface charge, and coating of the nanoparticles. The manipulation of these properties and an understanding of their effects play an important role in the improvement of the biodistribution and intracellular fate of the nanoparticles.

2.1 Size Distribution

Most biomedical applications require a size smaller than 100 nm and a narrow particle size distribution in order to evade the reticuloendothelial system [17]. The size and size distribution of the nanoparticles will be mostly determined by the chosen synthesis procedure and the coating.

Numerous methods have been developed to synthesize magnetic nanoparticles for biomedical applications such as sonolysis, aerosol/vapor methods, electrochemical methods, flow injection syntheses, polyol methods, sol-gel reactions, hydrothermal and high-temperature reactions, reactions in constrained environments, and synthesis by coprecipitation [18].

The most commonly used method for the synthesis of magnetite nanoparticles is the coprecipitation of iron salts, [3, 19, 20]. The main advantage of this process is the large amount of magnetite nanoparticles that are obtained in a simple and efficient chemical pathway. However, it has the disadvantage of affording limited control in particle size distribution. Figure 2.a shows a transmission electron micrograph (TEM) of magnetite nanoparticles obtained by the co-precipitation method in which the poor control in size and size distribution is evident.

On the other hand, nanoparticles with a high level of monodispersity and size control can be obtained by high-temperature decomposition of iron organic precursors, organic solvents, and surfactants [12]. A representative TEM image of nanoparticles obtained by the thermal decomposition method is shown in Figure 2.b.

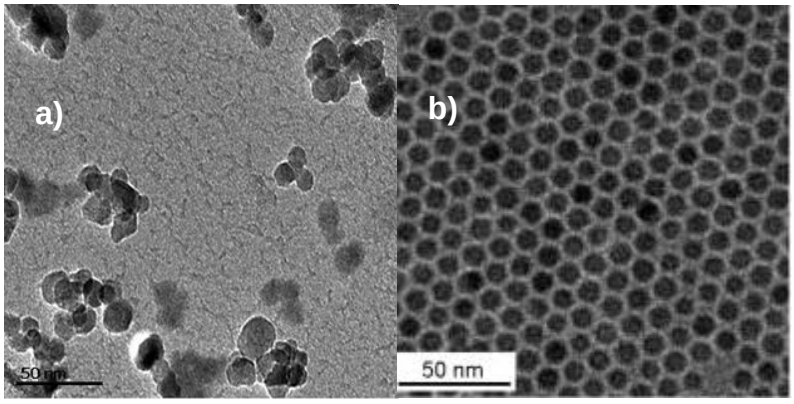

Figure 2. TEM of nanoparticles obtained by: a) co-precipitation method [24], b) thermal decomposition method [25].

2.2 Surface Modification

For *in vivo* applications, nanoparticles are usually used as magnetic fluids. In such applications the particles will be exposed to different pH and ionic strength conditions. For example, the pH inside tumor and inflamed tissues is approximately 6.8 while cellular compartments such as endosomes and lysosomes have a more acidic environment in a pH range of approximately 4-5. [47,48]. For this reason the modification of the magnetic nanoparticles is essential to obtain magnetic fluids which are stable against aggregation or precipitation in the biological medium. This stability results from the

equilibrium between attractive and repulsive forces such as van der Waals, magnetic dipolar forces, electrostatic forces, and steric repulsion forces in the case of coated particles [12]. Stabilization can be achieved through either electrostatic or steric repulsion forces. While steric repulsion forces depend on parameters such as molecular weight and the polymer density, the electrostatic repulsion is affected by the ionic strength and pH of the solution [12].

Commonly, a coating is used to prevent the agglomeration or aggregation of the particles, preferably stabilizing the suspension by steric repulsion. For this purpose, surfactant and polymer based coatings have been tested for biocompatibility. In the literature the most common coatings are polysaccharides, such as chitosan [18] and starch [21], dextran [28] , and derivatives of dextran [29] and other synthetic polymers such as polyethylene glycol [17], and polyethylene oxide [22]. Among these, dextran has proven to fulfill such requirements with no measurable reported toxicity index [23]. In fact, the Food and Drug Administration approved the use of superparamagnetic iron oxide nanoparticles as contrast agents for magnetic resonance imaging (MRI) [24]. These particles, called ferumoxides (e.g. Feridex I.V.), are dextran-coated magnetite nanoparticles with a mean hydrodynamic size of ~141 nm and a polydispersity index of 0.285 [25], which are obtained from a reaction of ferric chloride and ferrous chloride in the presence of ammonia [26].

Studies related to particle stability with dextran coatings have been performed. Xu *et al.* [27] studied the adsorption process of different dextran molecules onto the surface of magnetite nanoparticles suspended in water. The particles were obtained by a one step coprecipitation method in which the dextran solution was added during the nanoparticle

synthesis. They suggested that the adsorption of dextran to the nanoparticle surface was a physisorption process and that the particles were mainly stabilized by steric repulsion, judging from their weak negative charge. They showed that the adsorption of dextran at magnetite nanoparticle surfaces increased with increase in adsorption time, reaction temperature, and the mass ratio of dextran to magnetite. Dextran with a lower molecular weight showed better adsorption. TEM images demonstrated aggregation of the nanoparticles which indicates that the particles were not completely stable in water. Stability as a function of pH or ionic strength was not studied.

Kawaguchi *et al.* [28] studied the conformation of dextran chains and stability in solution of a dextran-magnetite complex. In this study alkali treated dextran, which has a carboxyl group at the reduction end, binds to a magnetite core by the linkage between the carboxyl group and an iron atom on the core surface. Dextran-magnetite particles were synthesized in a one step method in which an iron salt solution was added to a solution of alkali-treated dextran under an inert atmosphere and strong basic conditions, followed by reflux for 1 h at 100 º C and pH 7. Stability of dextran-magnetite solution was examined at 20˚ C and 80˚ C for a concentration of 2 mg Fe/ml in water. At 20˚ C no precipitation or aggregation was observed for at least six months. However at 60˚ C aggregation or precipitation was observed within two weeks. No change in the stability was observed by addition of NaCl at a concentration of 0.15. The stability as a function of pH was not considered. The stability of the dextran-magnetite complex was found to increase by increasing the molecular weight of dextran. Because in this case the dextran is not covalently attached, dissociation of dextran from the magnetite core occurred and could have caused the aggregation and/or precipitation of the particles.

Mornet *et al.* synthesized magnetic nanoparticles based on maghemite cores stabilized with covalently bonded dextran macro molecules. Magnetite nanoparticles were synthesized by the coprecipitation method and then oxidized to maghemite. A cationic maghemite ferrofluid was obtained by peptization with nitric acid. The maghemite nanoparticles were modified with 3-aminopropyltrimethoxysilane (APS) and then coated with partially oxidized dextran covalently attached to the APS molecule. In this process the mechanism of particle stability changes from electrostatic repulsion to steric repulsion due to the dextran coating. No aggregation or precipitation of the particles was reported, but stability against changes in pH or ionic strength was not studied.

Herrera *et al.* [29] functionalized magnetite nanoparticles obtained by co-precipitation with carboxymethyldextran covalently attached to the particles to prevent desorption of dextran chains. In this case, carboxylic groups present in the carboxymethyldextran molecule were activated and reacted with amine end groups previously grafted onto the nanoparticle surface by condensation of aminopropylsilane molecules. Colloidal stability was analyzed at different pH and NaCl concentrations. Highly stable suspensions of magnetite nanoparticles with electrostatic and steric repulsion and no particle precipitation at the studied pH range and ionic strength were reported.

Other researchers have used dextran or carboxymethyl dextran coated nanoparticles obatained by coprecipitation techniques to study nanoparticle-cell interaction and nanoparticle uptake [30]-[31]. In those studies the particles were suspended in culture medium (e.g. DMEM, RPMI-1640) with buffers such as phosphate-buffer saline and other additives. Tables 1 and 2 summarize the inorganic salt contents of

different formulations of DMEM and RPMI-1640, respectively. No particle aggregation or precipitation was reported in those studies, however, neither were detailed stability analyses reported.

Table 1. Inorganic salt content of different formulations of DMEM as reported by Sigma Aldrich.

INORGANIC SALTS	**D 0422**		**D 2429**	**D 2554**					
	RE	**D 1152**	**[10X]**	**[10X]**	**D 2902**	**D 3656**	**D 5030**	**D 5280**	**D 5523**
	g/L	**g/L**	**g/L**	**g/L**	**g/L**	**g/L**	**g/L**	**g/L**	**g/L**
CaCl2•2H2O	0.265	0.265	0.265	0.265	0.265	0.265	0.265	0.265	0.265
Fe(NO3)3•9H2O	0.0001	0.0001	0.0001	0.0001	0.0001	0.0001	0.0001	0.0001	0.0001
MgSO4	0.09767	0.09767	0.09767	0.09767	0.09767	0.09767	0.09767	0.09767	0.09767
NaHCO3	3.6	—	—	—	—	—	—	—	—
KCl	0.4	0.4	0.4	0.4	0.4	0.4	0.4	0.4	0.4
NaCl	6.4	6.4	6.4	6.4	6.4	6.4	6.4	6.4	6.4
NaH2PO4	0.109	0.109	0.109	0.109	0.109	0.109	0.109	0.109	0.109
Succinic Acid	—	—	—	—	—	—	—	0.075	—
Sodium Succinate	—	—	—	—	—	—	—	0.1	—

Table 2. Inorganic salt content of different formulations of RPMI-1640 as reported by Sigma Aldrich.

INORGANIC SALTS	**R 6504**	**R 8758**		**R 7388**
	R 5382	**[1X]**	**R 4130**	**[1X]**
	g/L	**g/L**	**g/L**	**g/L**
Ca(NO3)2•4H2O	0.1	0.1	0.1	0.1
MgSO4 (anhyd)	0.04884	0.04884	0.04884	0.04884
KCl	0.4	0.4	0.4	0.4
NaHCO3	—	2.0	—	—
NaCl	6.0	6.0	6.0	6.0
NaH2PO4 (anhyd)	0.8	0.8	0.8	0.8

2.2.1 Biodistribution

The nanoparticle's coating will affect their biodistribution. Particles that have a largely hydrophobic surface are recognizable by the reticuloendothelial system (RES) due to the opsonisation process in which particles that are injected into the bloodstream are coated by components (i.e., proteins) of the circulation [32]. In contrast, particles with a more hydrophilic surface can resist the opsonisation process, thus evading the RES, and have been shown to be cleared more slowly [33]. In this respect, dextran has proven to be long circulating [30]. For example, Feridex I.V. (i.e. ferumoxides) has a half life of 2.4 hours and are completely cleared from the blood 25 hours after administration [26] .

Although the interaction and distribution of nanoparticles will depend on cell type [34], the coating plays a vital role in the cell-particle interaction as shown by several studies. For example, Zhang *et al*. [35] used magnetite nanoparticles coated with poly(ethylene glycol) (PEG), folic acid (FA), and their conjugate PEG-FA to compare their effects on the improvement of intracellular uptake of the nanoparticles to human breast cancer cells, BT-20. Results obtained from cell culture experiments showed that the PEG-FA coated nanoparticles were internalized into BT-20 cancer cells and exhibited higher efficiency of intracellular uptake than nanoparticles coated only with PEG or FA.

C. Berry *et al*. [32] used magnetic nanoparticles derivatized with dextran and albumin to study the influence of the particle and coating on the cell-particle interaction in fibroblasts in vitro. The results for derivatized particles were compared with those for underivatized particles. In this case underivatized nanoparticles showed massive internalization which resulted in cell death. Dextran coated nanoparticles followed a similar internalization pattern. Although there was also evidence that albumin coated

particles were internalized, it did not appear to be at the same rate as dextran coated or underivatized nanoparticles. Further experiments by C. Berry *et al*. [36] showed similar results. In this study only uncoated and dextran coated nanoparticles were studied and both showed a similar uptake level.

2.3 Surface Charge

Another factor that affects cell-particle interaction and intracellular uptake is surface charge. The nanoparticle surface can be positive, neutral, or negative. Some studies have been done regarding the effects of surface charge on uptake of nanoparticles and their interaction with cells. C. Wilhelm *et al*. [37] studied the intracellular uptake of anionic maghemite nanoparticles as a function of their surface coating. The maghemite nanoparticle's negative charge was due mainly to unbound carboxylate groups from the chelating agent meso-2,3-dimercaptosuccinic acid (DMSA). The average diameter of maghemite nanoparticles was 3-5 nm as obtained by TEM. To evaluate the role of the surface coating on cell uptake, cell uptake assays were also done for dextran-magnetite nanoparticles (Ferumoxtran) obtained from Advanced Magnetics Inc. For dextran-coated nanoparticle the average diameter obtained by TEM was 5 nm for the magnetite cores; however dextran with an average chain length of 20 nm was used for the coating, which should result in a greater hydrodynamic diameter. The hydrodynamic diameter for the DMSA or dextran coated nanoparticles was not reported. They showed that anionic nanoparticles strongly interacted none specifically with the plasma membrane and were captured by HeLa cells with an efficiency three orders of magnitude higher than dextran-coated nanoparticles. They attributed this observation to the negative surface charge of the particles and hypothesized that electrostatic interactions govern the adsorption

process. Although it is known that the plasma membrane is mainly negatively charged with only few cationic sites, they suggested according to TEM images, that anionic nanoparticles bind to the cell surface in the form of clusters presumably on the positively charged sites due to their repulsive interaction with the negatively charged cell surface. This aggregation of particles preceded the internalization. The overall process is named adsorptive endocytosis. For dextran coated nanoparticles the difference in uptake was related to the lack of binding of dextran nanoparticles on the plasma membrane which inhibits the adsorptive endocytosis and limits internalization to fluid phase endocytosis. However, due to the potentially large difference in particle diameter, particle uptake could have been significantly affected by a size effect.

Pallab *et al.* [23] studied the cellular interactions of lauric acid coated and dextran coated magnetite nanoparticles in mouse fibroblast and human cervical carcinoma cell lines. Their results showed that lauric acid coated nanoparticles were less cytocompatible than the dextran coated nanoparticles and cellular uptake of lauric acid coated nanoparticles was higher than for dextran coated nanoparticles. Lauric acid coated nanoparticles are anionic in nature due to the carboxylate groups present in the nanoparticles' surface, while dextran coated nanoparticles are neutral due to the lack of charge in the dextran molecule. For instance, they attributed the difference in uptake of lauric acid coated nanoparticles to the electrostatic interactions using the argument by C. Wilhelm *et al*. [37] However, it must be recognized that for lauric acid coated nanoparticles the lauric acid forms a surfactant double layer. This gives the particles a hydrophobic character. Furthermore, desorption of the outer surfactant layer can result in aggregation, confusing the results.

Other researchers have studied the effect of positive surface charge on the cellular uptake of nanoparticles. For example Daniel *et al*. [38] evaluated the cellular uptake of superparamagnetic iron oxide nanoparticles in non-phagocytic T cells. Magnetite nanoparticles were synthesized by the co-precipitation method and coated with dextran followed by crosslinking and amination of the dextran chain with epichlorohydrin and ammonium. They manipulated the surface charge by amine-blocking of particles with glycidol, thus obtaining nanoparticles with different positive charges. Under their experimental conditions it was found that the particles in their natural, fully aminated state were maximally internalized.

On the other hand, Myriam *et al*. [39] studied the uptake of functionalized, fluorescent-labeled polymeric particles in various cell lines (i.e., HeLa, Jurkat, and KG1a) and stem cells (i.e., mesenchymal stem cell). Polymeric particles were synthesized by a miniemulsion process which they claimed yields submicron-sized particles of narrow size distribution, although no particle size characterization was reported. They controlled the surface charge by adjusting the amount of a copolymerized monomer with amino groups. Although the amine groups per particle were calculated no zeta potential measurement was reported and the monomer used was not specified. Fluorescent-activated cell sorter measurements were used to study cellular uptake. For HeLa, Jurkat, and KG1a cell lines results showed a correlation between surface charge and fluorescence intensity. As the positive surface charge increased the fluorescence intensity increased, being smallest for neutral nanoparticles.

As a final example; Shinkai *et al.* [40], developed magnetite cationic liposomes and compared them to neutrally charged liposomes. In this case the cationic liposomes

showed a 10-fold higher affinity for rat glioma cells compared to the neutral liposomes, as evidenced by the internalization of the cationic liposomes.

Previous studies suggest that there is an effect of surface charge on the uptake and interaction of nanoparticles. However, these studies compare uncoated versus coated nanoparticles, neutral versus negatively charged nanoparticles with different coatings for each case, or neutral versus positively charged nanoparticles. In addition the difference in coating in some cases resulted in a difference in particle size. In such comparisons it is impossible to attribute the differences in uptake to surface charge alone. In addition, although dextran and carboxymethyl dextran coated nanoparticles are widely used, the effect of surface charge on internalization of carboxymethyl dextran coated nanoparticles has not been studied. Recognizing the important role that surface charge may play in cellular uptake and particle cell interaction, the present work aims to obtain carboxymethyl dextrans with different degrees of substitution. These carboxymethyl dextrans will be used for magnetite nanoparticle funtionalization and the surface charge will be analyzed.

3 MATERIALS AND METHODS

3.1 Materials

Iron (III) chloride hexahydrate 97%, oleic acid, chloroacetic acid 99+% A.C.S reagent (MCA), dextran, 1-ethyl-3-(3-dimethylaminopropyl) carbodiimide hydrochloride (EDC), N-hydroxysuccinimide (NHS) 98%, acetic acid 99.7%, and fluorescein-amine isomer I, dulbecco's modified eagle's medium (DMEM), and Hank's balanced salt solution (HBSS) were purchased from Sigma Aldrich (St. Louis, MO). 3-Aminopropyltriethoxysilane (APS) and sodium oleate were obtained from TCI America (Portland, OR). 1-octadecene was obtained from Alfa-aesar (Ward Hill, MA). Hexane and Ethanol anhydrous were purchased from Fisher Scientific (Pittsburgh, PA). All reagents were used as received. A number average molecular weight of 10 kDa with a polydispersity index of 1.2 was obtained for native dextran by gel permeation chromatography (GPC) using a Brookhaven Instruments molecular weight analyzer BI-MwA and a PLaquagel-OH Mixed 8 μm column.

3.2 Synthesis of Carboxymethyl Dextran

Carboxymethyl dextran (CMDx) was prepared by carboxymethylation reaction in which monochloro acetic acid reacts with dextran in the presence of sodium hydroxide [41, 42], as shown in Figure 3. The degree of carboxymethylation was controlled by adjusting the sodium hydroxide concentration. For this, 5 g of dextran were dissolved in 25 ml of distilled water. Sodium hydroxide (NaOH) was dissolved in 17 ml of distilled water, for a final concentration of 1M, 2M or 3M. NaOH concentration was calculated

using total reaction volume. The solutions were cooled in an ice bath and the NaOH was added drop wise to the dextran solution at approximately 4 ºC over 20 minutes. Then, 7.29 g of solid monochloro acetic acid were slowly added and manually stirred allowing it to dissolve in the solution. The reaction mixture was placed in a water bath with shaker at 100 rpm and 60 ºC for 75 minutes. After the reaction, the mixture was allowed to reach room temperature before neutralization with glacial acetic acid. Finally, the product was precipitated and washed twice with ethanol, dialyzed to a conductivity of ≤ 6 µS /cm, concentrated using a Brinkmann RE 121 rotary evaporator and dried at 60 ºC. The dried sample was powdered and stored.

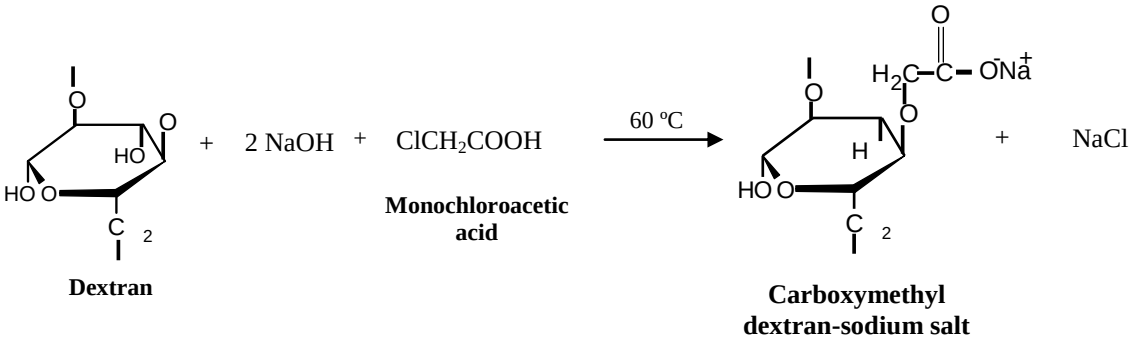

Figure 3. Carboxymethylation reaction.

3.3 Characterization of CMDx

The synthesized CMDx is obtained in the form of a sodium salt (i.e., carboxylate). In order to accurately determine the degree of substitution (DS) of the –COOH groups it is necessary to convert the CMDx completely to the free acid form by washing it with an acid reagent, followed by acidimetric titration [43]. For this, 1 g of CMDx was washed overnight with 14 ml of a solution of anhydrous methanol and nitric acid 70 %v/v (10:1).

The acid liquor was removed by vacuum filtration and the CMDx was subsequently washed several times with ethanol to remove all traces of the acid reagent, and dried in a vacuum oven at 60 ºC.

A solution at 1% w/v of the CMDx in free acid form was prepared in a 1:1 distilled water/acetone mixture and 5 ml to 10 ml of NaOH 0.0121 N were added. This solution was titrated with hydrochloric acid 0.0121 N, using phenolphthalein as indicator. From the titration data, the miliequivalents of -COOH groups per gram of sample (A) was calculated as according to [43]:

$$A = \frac{\left(Ml.\ of\ \ NaOH * [NaOH](mol/L)\right) - \left(Ml.\ \ HCl * [HCl](mol/L)\right)}{grams of\ CMD\ sample} \quad . \qquad (3.1)$$

The DS, which is defined as the average number of sodium carboxy methyl groups per anhydroglucose unit, is calculated from [41]

$$DS = \frac{0.162(A)}{1 - 0.08(A)}, \qquad (3.2)$$

where 0.162 is the molecular weight of an anhydroglucose unit and 0.08 is the molecular weight of the substituent group (-CH_2COONa), both corrected for units. The DS is related to the number of –COOH groups per dextran chain as follows

$$\frac{-COOH}{Dextran\ \ chain} = \frac{Mw\ of\ \ Dextran}{Mw\ of\ \ anhydroglu\cos e\ unit} * DS \quad . \qquad (3.3)$$

3.4 Synthesis of magnetite nanoparticles functionalized with APS

Magnetite nanoparticles coated with oleic acid were synthesized by the thermo-decomposition method from an iron oleate solution using 1-octadecene as solvent [44]. The iron oleate solution was obtained after reaction of 3.24 g of the iron (III) salt and 10.95 g of sodium oleate in 96 ml of a mixture formed by distilled water/ethanol/hexane (1:1:2) at 70 °C with reflux for 4 h. Afterwards, the iron oleate was washed three times with distilled water using a separation funnel and then dried at 80 °C.

Magnetite nanoparticles were synthesized using 10 g of the dried iron oleate solution suspended in 56 g of 1-octadecene with the addition of 1.6 g of oleic acid. Synthesis was carried out at 320 °C with a heating rate of 3.3 °C/min in a vessel reactor with a reflux condenser and mechanical agitator run at 100 rpm. Nanoparticles were allowed to grow for 30 min at 320 °C. Afterwards, the reaction mixture was cooled to room temperature and washed with ethanol (1:4) at 7500 rpm for 15 min. Magnetite-oleic acid nanoparticles were suspended in hexane and centrifuged at 2000 rpm for 10 min, obtaining a stable colloid.

Functionalization of magnetite-oleic acid nanoparticles with amine-silane (APS) molecules was performed via ligand exchange in presence of acetic acid [45]. In a typical functionalization, 6 ml of APS and 50 μL of acetic acid were added to 115 ml of a colloid formed by magnetite-oleic acid nanoparticles suspended in hexane. This functionalization was mechanically stirred at room temperature for three days. Afterwards, magnetite-APS nanoparticles were washed three times with 50 ml of hexane and then once with 20 ml of diethyl ether and dried at room temperature.

The size of the synthesized magnetite-oleic acid and the modified magnetite-APS nanoparticles were determined by TEM measurements.

3.5 Coating of magnetite-APS nanoparticles with fluorescent CMDx

Fluorescent magnetite nanoparticles were prepared by incorporation of fluorescein-amine to the CMDx chains, prior to the coating process. For this purpose, 50 mg of fluorescein-amine were suspended in 5 ml of ethanol and cooled to 4 °C for 30 min. This fluorescent solution was reacted with 10 ml of an aqueous CMDx solution prepared at 0.013 M with the addition of 25 mg of EDC at pH 5.0 and previously cooled to 4 °C for 30 min. This reaction mixture was mechanically stirred at room temperature for three days. Afterwards, free fluorescent molecules were removed by washing with ethanol and centrifuging at 8000 rpm for 30 min until a clear supernatant was obtained.

The fluorescent-CMDx molecules were used to coat magnetite-APS nanoparticles by carbodiimide activation, forming a chemical bond between carboxylic (–COOH) groups present in the CMDx chains and amine ($–NH_2$) groups previously grafted onto the magnetite nanoparticles [29]. For this purpose magnetite-APS nanoparticles were suspended in 10 ml of deionized water at 2.0 % w/v and pH 5.0 using HNO_3 1M. A CMDx solution was prepared in 10 ml of deionized water at 0.013 M and pH 5.0 with the addition of 25 mg of EDC and 15 mg of NHS. Magnetite-APS nanoparticle solution was mixed with the activated CMDx solution and then reacted at room temperature for 36 h. Afterwards, free CMDx molecules were removed by washing the functionalized nanoparticles three times with ethanol (1:3) at 8000 rpm for 15 min.

This procedure was followed for each of the CMDx synthesized.

3.6 Transmission Electron Microscopy (TEM)

The size of the synthesized magnetite-oleic acid, the modified magnetite-APS nanoparticles, and the CMDx coated magnetite-APS nanoparticles were determined by TEM measurements using a JEOL 1200EX and the ImageJ program (distributed by NIH) to measure the diameters of one hundred nanoparticles, which were analyzed using a lognormal distribution.

For this, samples of magnetite nanoparticles coated with oleic acid and suspended in hexane, magnetite-APS nanoparticles suspended in deionized water at pH 5.0, and magnetite-APS-CMDx nanoparticles suspended in deionized water at pH 7.0 were prepared. Then, ultra thin carbon type A grids were immersed in the nanoparticle solutions, placed on filter paper and dried in a vacuum oven for 30 min.

3.7 Characterization of CMDx and magnetite-CMDx nanoparticles

Fourier Transform Infrared (FTIR) spectra were acquired using a Varian 800 FTIR and a ZnSe ATR holder with a wavenumber range from 600 to 4000 cm^{-1}. Hydrodynamic diameter and zeta potential of fluorescent magnetite nanoparticles were measured using a Brookhaven Instruments BI-90 Plus Particle Size and Zeta Potential Analyzer.

4 RESULTS AND DISCUSSION

The nanoparticle surface charge can be tailored by controlling the charged groups in the coating material. For this reason, we studied the addition of carboxymethyl groups into the dextran molecule by carboxymethylation reaction and its effects on the nanoparticle's surface charge and stability.

4.1 Characterization of carboxymethyl dextran

The carboxymethylation reaction was performed by treating a solution of dextran in water with monochloroacetic acid and sodium hydroxide [42]. According to the literature the degree of substitution (DS) depends on reaction parameters such as solvent, sodium hydroxide concentration, MCA/dextran ratio, temperature and duration of the reaction and the number of carboxymethylation steps [41]. For instance we varied reaction parameters to obtain four different degrees of substitutions as shown in Table 3. However the CMDx 2 obtained was insoluble in water and could not be used for the functionalization of the nanoparticles. Carboxylic groups in the dextran molecule may form lactones when complete neutralization or an acid pH is promoted in the obtained CMDx solution after reaction [49]. Since the concentration of NaOH used in this reaction is low, the MCA is not neutralized and the resulting solution is acidic, probably promoting lactone formation. As a result a carboxymethyl dextran with lactones groups may be formed, a product that has been observed to have a low water solubility [50].

Among the evaluated parameters, the sodium hydroxide concentration and the number of carboxymethylation reactions were the parameters that most affected the degree of substitution (Appendix A).

Table 3. Summary of carboxymethylation reaction conditions and results.
5.0 g dextran, 7.28 g MCA, 42 ml water (total volume), 60º C, mechanical agitation at 100 rpm, 75 min reaction.

CMDx	[NaOH]	Reaction Steps	DS	-COOH groups per dextran chain
CMDx-2	1M	1	0.03	2
CDMx-5	2M	1	0.08	5
CMDx-23	3M	1	0.38	23
CMDx-38	3M	2	0.61	38

As mentioned in the previous chapter, carboxymethyl dextran was obtained from the carboxymethylation reaction as a sodium salt, which also may contain some carboxylic groups in free acid form. These groups can be imperceptible in the FTIR spectra due to their small quantity relative to other functional groups. To accurately quantify the number of carboxymethyl groups introduced into the dextran molecule a washing procedure using methanol acidified with nitric acid was performed. In this process all the carboxymethylated groups (-CH_2COONa) were converted to the free acid form (-CH_2COOH). The effectiveness of the carboxymethylation reaction and the washing procedure was first qualitatively evaluated by Fourier Transform Infrared (FTIR) spectroscopy. Figures 4 to 6 illustrate the results for three different carboxymethyl dextrans synthesized, named CMDx 5, CMDx 23, and CMDx 38, respectively. In this notation the numbers represent the amount of carboxymethyl groups that were introduced into the dextran molecule. In each figure we can observe in (a) the spectrum of dextran prior to carboxymethylation reaction, in (b) the spectra of the carboxymethyl dextran in carboxylate form and in (c) the spectra of the carboxymethyl dextran after the acid wash

procedure. The observed bands at 1588-1592 cm $^{-1}$ are attributed to antisymmetric CO_2 stretching in carboxylic acid salts [46], which indicate that the introduction of carboxymethyl groups into the dextran was successful. As can be observed in the figures, the intensity of the bands is directly related to the amount of carboxymethyl groups in the dextran molecule. In curve (b) of Figure 4, an almost imperceptible band at 1734 cm $^{-1}$ appears, which is attributed to carboxylic acid groups in free acid form. These observations corroborate the necessity of the acid wash procedure. In curve (c) of Figures 5 and 6 bands at 1734-1737 cm $^{-1}$, are attributed to the carboxylic acid groups in free acid form. In the case of CMDx 5 the curve (c) which corresponds to the CDMx 5 in free acid form does not present the expected band at near 1734 cm $^{-1}$, which is probably due small signal intensity.

For the quantitative determination of the number of carboxymethyl groups introduced to the dextran molecule an acid-base titration was performed to the carboxymethyl dextran in free acid form, as described in the previous chapter. The degree of substitution (DS) and the number of carboxymethyl dextran groups were calculated using the titration data, and the results are summarized in Table 3.

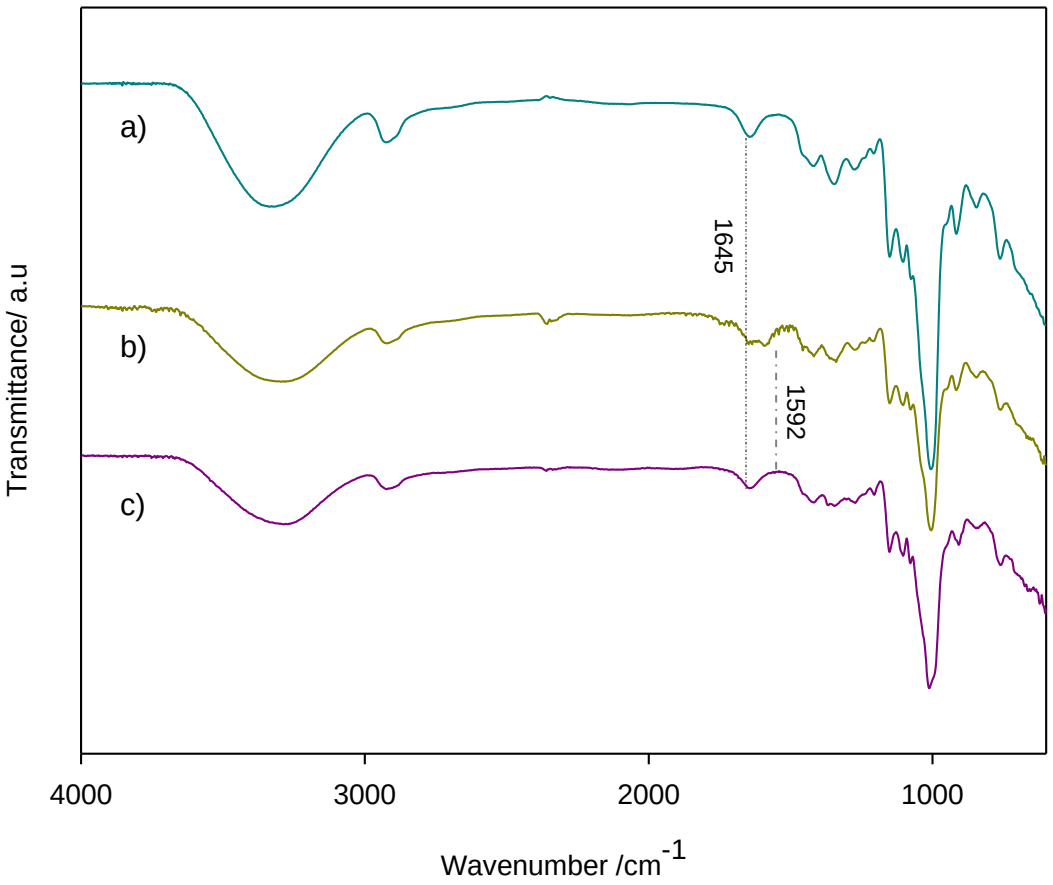

Figure 4. FTIR spectra of a) Dextran, b) CMDx 5 in carboxylate form and c) CMDx 5 in free acid.

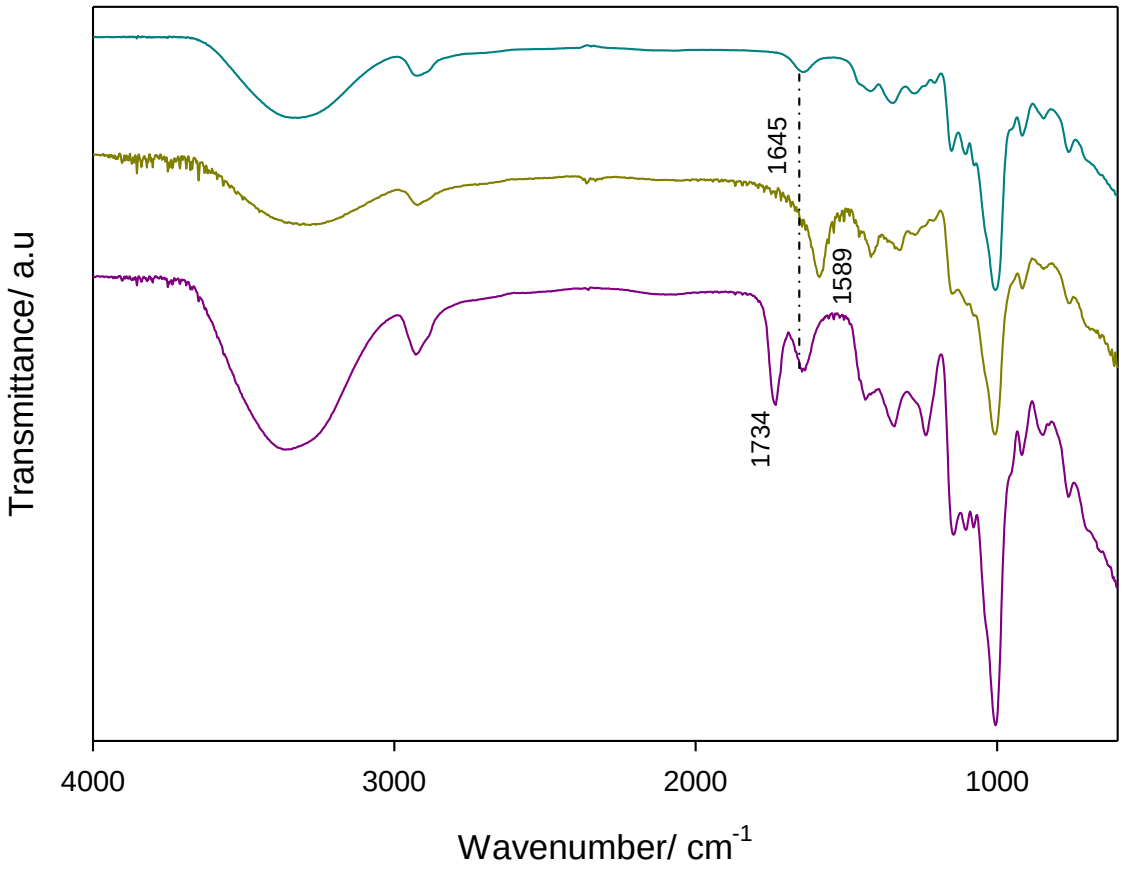

Figure 5. FTIR spectra of a) Dextran, b) CMDx 23 in carboxylate form and c) CMDx 23 in free acid form.

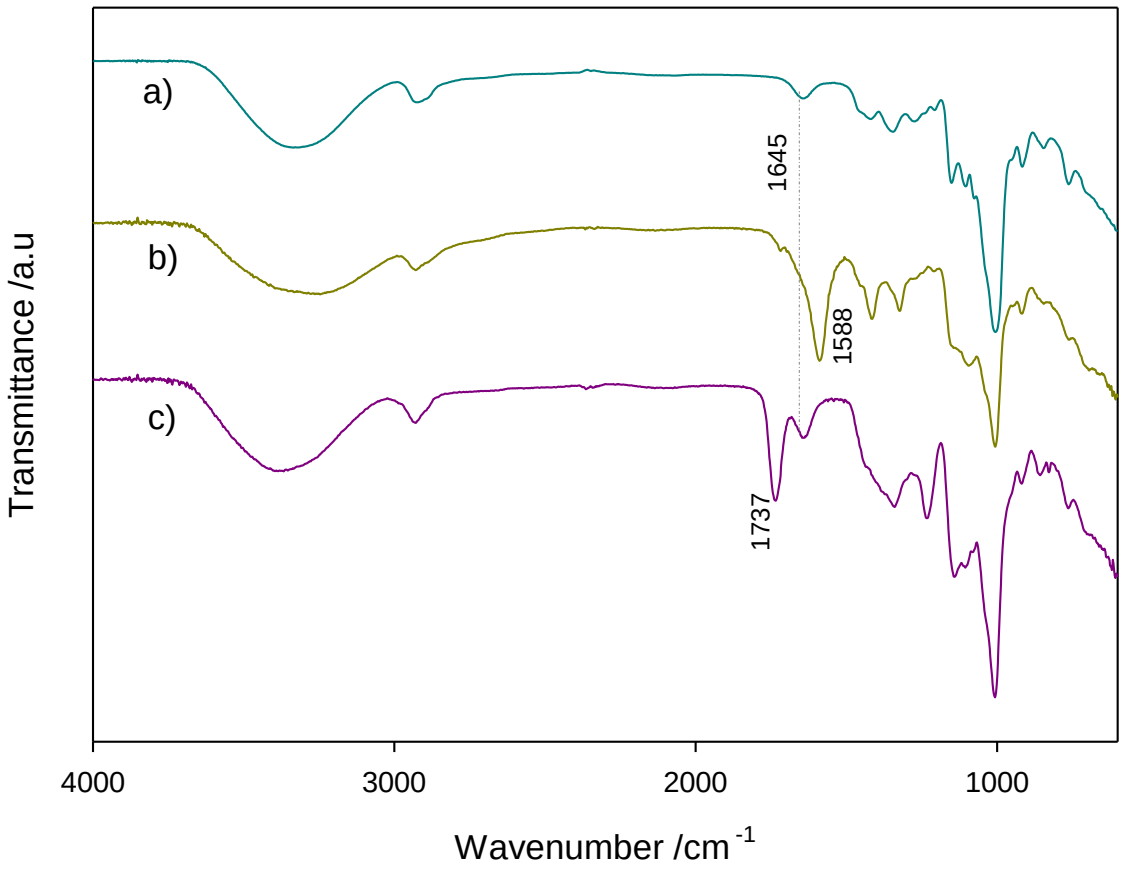

Figure 6. FTIR spectra of a) Dextran, b) CMDx 38 in carboxylate form and c) CMDx 38 in free acid form.

4.2 Characterization of Magnetite-APS-CMDx nanoparticles by Fourier Transform Infrarred (FTIR) Spectroscopy

Magnetite nanoparticles were synthesized by the thermo-decomposition method, funtionalized with APS molecules, and coated with different carboxymethyl dextrans. The functionalization of magnetite nanoparticles with both APS and CMDx was examined by FTIR spectroscopy, as shown in Figure 7. Curve (a) presents the spectrum of magnetite nanoparticles coated with APS for which we can observe the characteristics bands for APS. The bands at 2928, 1486 ad 1328 cm^{-1} are characteristic of the asymmetric $–CH_2$ stretching, $-CH_2$ deformation and –CH deformation, respectively [46]. Vibrational modes at 3400, 1627, 1556 and 873 cm^{-1} correspond to the –N-H stretching vibration, $-NH_2$ bending of free amino groups, C-H stretching and NH_2 wagging, respectively [46]. Bands at 1108 and 1000 cm^{-1} are attributed to the Si-O-Si bonds formed by the oligomerization of siloxane groups [29]. Curves (b) to (d) in Figure 7 present the spectrums for magnetite-APS-CMDx nanoparticles for the three different CMDx used. In these curves the bands between 2919-2927 cm^{-1} and 3328-3400 cm^{-1} correspond to the asymmetric CH_2 stretching and N-H stretching, respectively [46]. Peaks at 1588 cm_{-1} and 1154-1156 cm_{-1} are characteristic of the C(=O)-N-H secondary amine bond and the antisymmetric stretch of the C-N-C secondary amine moiety, respectively [29]. These peaks corroborate the formation of the bond between the carboxylic group and the amine groups present in the nanoparticle. The peaks at 914-916 and 847 cm^{-1} correspond to the α-glucopyranose ring of the CMDx molecule; and peaks at 1409-1417

cm^{-1} and 1004-1009 cm^{-1} are attributed to the $-CH_2$ deformation and C-O groups in the CMDx molecule [29].

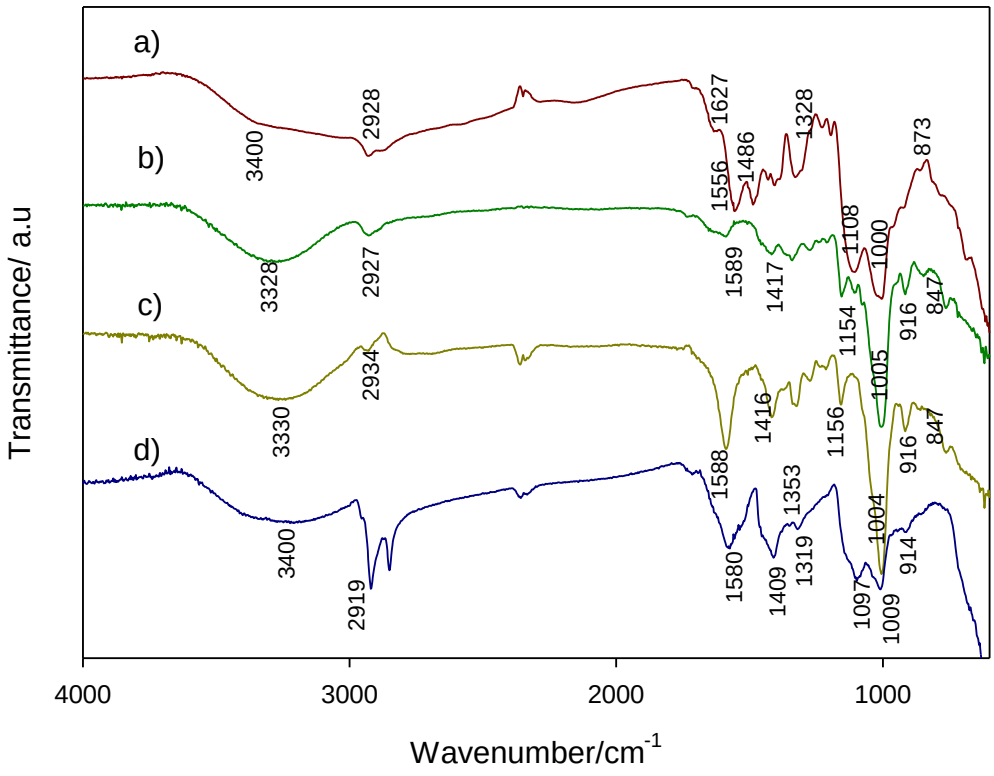

Figure 7. FTIR spectra of a) magnetite nanoparticles functionalized with APS, b) magnetite-APS nanoparticles coated with CMDx 5 c) magnetite-APS nanoparticles coated with CMDx 23, and d) magnetite-APS nanoparticles coated with CMDx 38.

4.3 Transmission Electron Microscopy (TEM)

The size of the synthesized magnetite-oleic acid nanoparticles suspended in hexane and the modified magnetite-APS and magnetite-APS-CMDx nanoparticles suspended in deionized water were determined by TEM measurements. Figure 8 illustrates these measurements from which we have determined a nanoparticle size of 13 nm with a geometric deviation σ_g of 0.1 for magnetite nanoparticles coated with oleic acid. No agglomeration was observed after ligand exchange with APS.

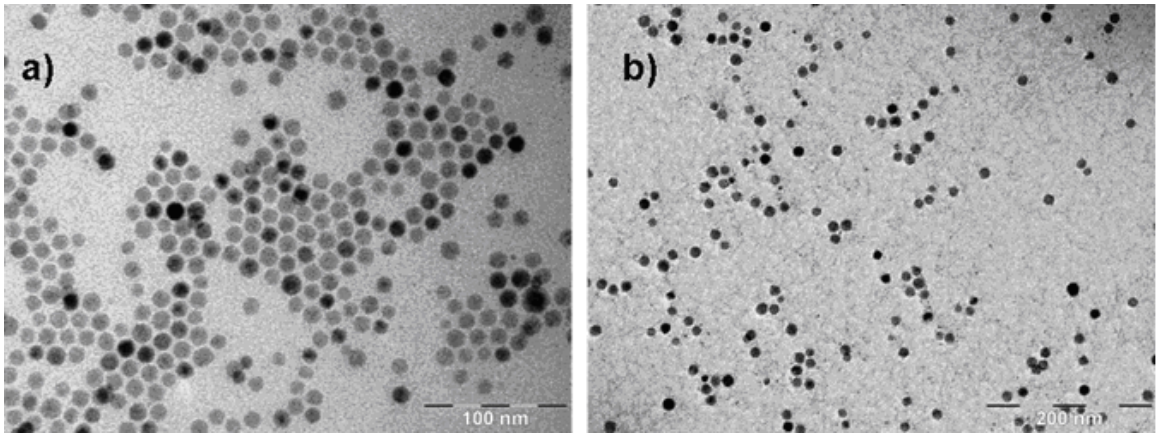

Figure 8. TEM measurements of magnetite nanoparticles. a) Magnetite nanoparticles coated with oleic acid, and b) magnetite nanoparticles functionalized with APS after ligand exchange.

4.4 Surface charge and particle stability

Particle stability was studied as function of pH and ionic strength for the three CMDx synthesized. In this study particle stability implies that no particle aggregation or precipitation was observed over a pH range from 2.0 to 10.0 and a sodium chloride (NaCl) concentration from 0 to 0.1380 M NaCl. We used DLS to measure the hydrodynamic size of the CMDx functionalized nanoparticles as a function of pH and

ionic strength. The values of hydrodynamic diameters expressed in this section correspond to an average diameter. However for each measurement a size distribution was obtained and results are shown in Appendix B. In each plot of hydrodynamic diameter versus either pH or ionic strength, the error bars is calculated from the size distribution data.

A hydrodynamic size of 34.2 nm was determined for magnetite-APS-CMDx 5 suspended in distilled water at pH 7.2 and filtered with 0.2 μ nylon. For magnetite-APS-CMDx 23 the hydrodynamic diameter at pH 7.0 was 39.20 nm and for magnetite-APS-CMDx 38 was 43.1 nm. As shown in Figure 9, the hydrodynamic size for magnetite-APS coated with CMDx 5, CMDx 23 and CMDx 38 did not change significantly over the studied pH range, and no precipitation was observed. Two samples were analyzed for each type of particle and the same behavior was observed indicating that the results were reproducible. The particle's stability indicates that the bond between the CMDx chains and the APS molecules was formed and the particles were stabilized by steric repulsion, due to CMDx coating.

The hydrodynamic size of magnetite-APS-CMDx nanoparticles was also measured in the presence of NaCl. For these measurements a solution of magnetite-APS-CMDx nanoparticles at 0.5% w/v in 30 ml of deionized water at pH 7 with 0.3 ml of KNO_3 of 1.0 mM was prepared. Then, NaCl was added to the nanoparticle solution up to a concentration of 0.14 M. This concentration is greater than the concentration of NaCl in the culture medium which is approximately 0.1095 M. This was done to evaluate the stability of the particle at an ionic strength similar to that of the culture medium. Figure 10 shows these results, from which we can see that the hydrodynamic diameter did not

change significantly. Two samples were analyzed for each type of particle, obtaining similar behavior, indicating that the results were reproducible. In addition a sample of magnetite-ASP-CMDx 5 was sterilized at 120 º C for 1 hr and 50 mg were suspended in 5 ml of DMEM. A hydrodynamic diameter of 44.5 nm was measured immediately after preparation. The sample was then stored in the refrigerator at 8 ºC for one week. After this period the measured hydrodynamic diameter was 43.2 nm, which demonstrates that the particles are stable even after autoclave.

The surface charge and isoelectric point of the magnetite-APS-CMDx nanoparticles was studied by zeta potential measurements. In all zeta potential measurements two samples were analyzed obtaining similar behavior which shows reproducibility of the results. For this, a solution of magnetite-APS-CMDx nanoparticles at 0.5% w/v in 30 ml of deionized water with 0.3 ml of KNO_3 of 1.0 mM was prepared. The pH of the solution was then varied from 2 to 10.0, by titration with KOH and HNO_3. Results are presented in Figure 11. The isoelectric point was observed near pH 2 for all samples and is attributed to free carboxylic acid groups present in the nanoparticle surface, which also impart the observed negative charge. It is important to mention that the particles were stable in the whole pH range and no precipitation was observed. This observation suggests that nanoparticle stabilization occurred by steric repulsion. Also, we can observe that by decreasing the carboxylic group content the nanoparticle, surface charge significantly decreases without affecting stability. The isoelectric point of the magnetite-APS nanoparticles was observed near pH 10.0. The Magnetite-APS nanoparticles are not stable and precipitate at pH beyond ~6 due to the absence of steric repulsion.

The zeta potential of the magnetite-APS-CMDx nanoparticles was also measured with the addition of NaCl, to study the effect of ionic strength on surface charge and stability. The nanoparticle solution was prepared as in the previous case at pH 7.0, and NaCl was added up to a concentration of 0.14 M. Figure 12 illustrates the results, in which a considerable decrease in zeta potential is observed by increasing the NaCl concentration. For the case of magnetite-APS-CMDx 5 the zeta potential becomes positive at high ionic strength, which probably occurs due to adsorption of Na+ ions. The particles remained stable in the whole NaCl concentration range and no precipitation was observed during the time of the analysis, as demonstrated by the DLS measurements.

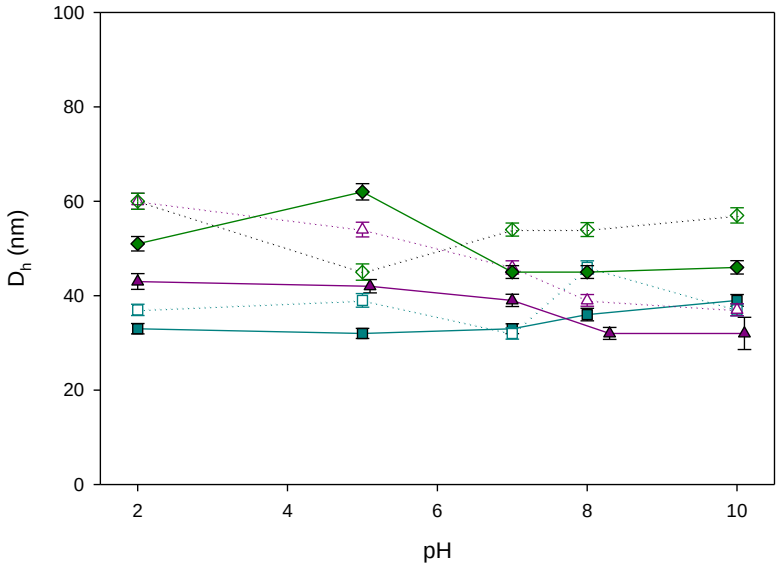

Figure 9. Nanoparticle hydrodynamic diameter as function of pH for two samples of magnetite-APS-CMDx 5 (closed and open squares), magnetite-APS-CMDx 23 (closed and open triangles) , and magnetite-APS-CMDx 38 (closed and open diamonds).

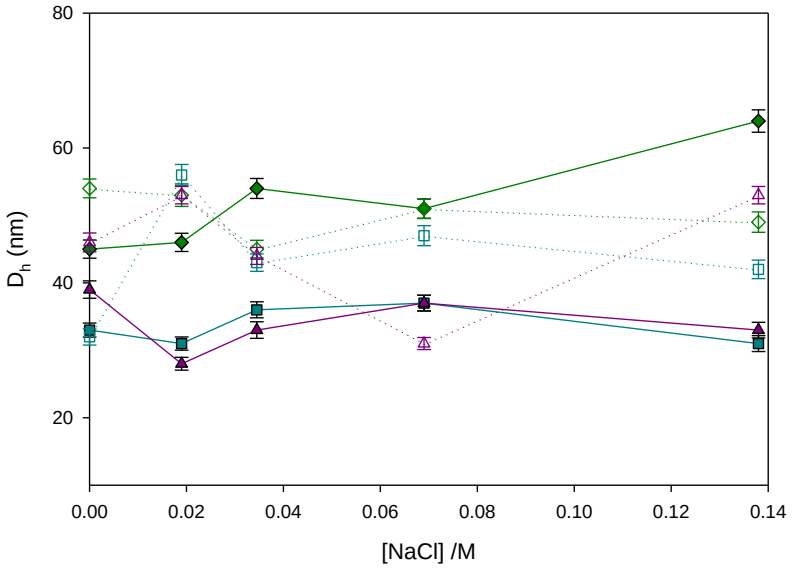

Figure 10. Hydrodynamic diameter as a function of NaCl concentration for for two samples of magnetite-APS-CMDx 5 (closed and open squares), magnetite-APS-CMDx 23 (closed and open triangles) , and magnetite-APS-CMDx 38 (closed and open diamonds).

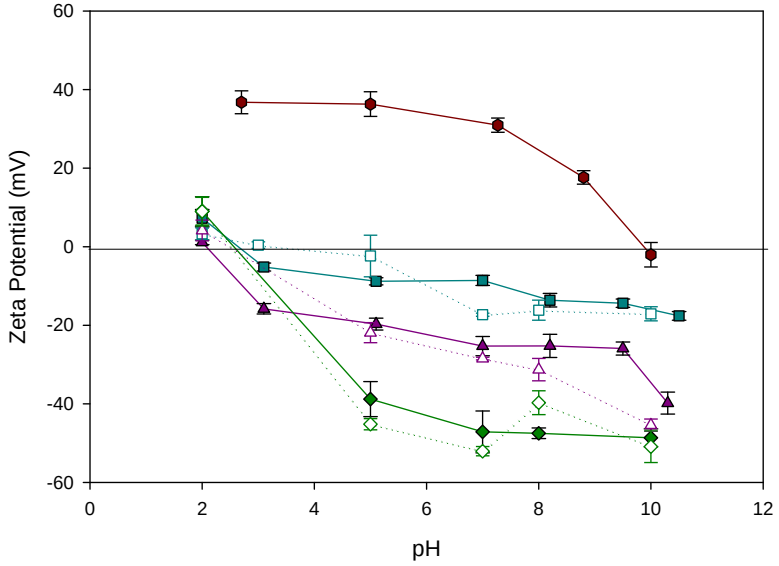

Figure 11. Zeta potential as function of pH for magnetite-APS nanoparticles (circles) , for two samples of magnetite-APS-CMDx 5 (closed and open squares), magnetite-APS-CMDx 23 (closed and open triangles) , and magnetite-APS-CMDx 38 (closed and open diamonds).

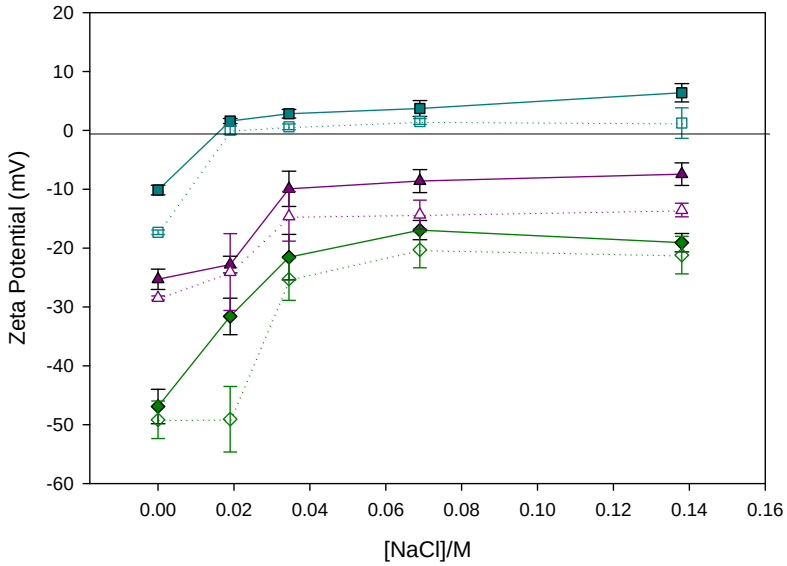

Figure 12. Zeta potential as function of NaCl for two samples of magnetite-APS-CMDx 5 (closed and open squares), magnetite-APS-CMDx 23 (closed and open triangles) , and magnetite-APS-CMDx 38 (closed and open diamonds).

5 CONCLUSIONS

Carboxymethyl dextrans with 2, 5, 23 and 38 –COOH groups per dextran chain were synthesized by a carboxymethylation reaction; however CMDx 2 was insoluble in water, and was not used in to functionalize nanoparticles. Different degrees of substitution were obtained by varying the sodium hydroxide concentration and the number of carboxymethylation reactions. Functionalization of magnetite nanoparticles with synthesized carboxymethyl-dextrans was performed by carbodiimide chemistry in which amine groups previously grafted onto the nanoparticles surface reacted with carboxylic groups (-COOH) present in the CMDx chain. The nanoparticle's surface charge was evaluated by zeta potentcial measurements as a function of pH and ionic strength. The stability of the particles was studied by measuring the nanoparticle's hydrodynamic diameter during the zeta potential analyses. The nanoparticles coated with CMDx with

5 –COOH, 23 –COOH, and 38 –COOH groups per dextran chain were stable over the entire pH range and NaCl concentration studied. With the obtained particles, we observe that the surface charge decreased significantly by decreasing the amount of –COOH groups without affecting the particle stability.

REFERENCES

[1] C. Phoenix, "History of Nanotechnology ", [Online]. Available: http://www.nanotech-now.com/Press_Kit/nanotechnology-history.htm.

[2] M. C. Roco, "Nanoparticles and nanotechnology research," *Journal of Nanoparticle Research,* vol. 1, pp. 1-6, 1999.

[3] D. K. Kim, M. Mikhaylova, Y. Zhang, and M. Muhammed, "Protective Coating of Superparamagnetic Iron Oxide Nanoparticles," *Chem. Mater.,* vol. 15, pp. 1617-1627, 2003.

[4] I. J. Bruce and T. Sen, "Surface Modification of Magnetic Nanoparticles with Alkoxysilanes and Their Application in Magnetic Bioseparations," *Langmuir,* vol. 21, pp. 7029-7035, 2005.

[5] C. Alexiou, R. Jurgons, R. Schmid, A. Hilpert, C. Bergemann, F. Parak, and H. Iro, "In vitro and in vivo investigations of targeted chemotherapy with magnetic nanoparticles," *Journal of Magnetism and Magnetic Materials,* vol. 293, pp. 389-393, 2005.

[6] J. L. Zhang, R. S. Srivastava, and R. D. K. Misra, "Core-shell magnetite nanoparticles surface encapsulated with smart stimuli-responsive polymer: Synthesis, characterization, and LCST of viable drug-targeting delivery system," *Langmuir,* vol. 23, pp. 6342-6351, 2007.

[7] F. H. Wang, I. H. Lee, N. Holmstrom, T. Yoshitake, D. K. Kim, M. Muhammed, J. Frisen, L. Olson, C. Spenger, and J. Kehr, "Magnetic resonance tracking of nanoparticle labelled neural stem cells in a rat's spinal cord," *Nanotechnology,* vol. 17, pp. 1911-15, 2006.

[8] Y.-M. Huh, E.-S. Lee, J.-H. Lee, Y.-W. Jun, P.-H. Kim, C.-O. Yun, J.-H. Kim, J.-S. Suh, and J. Cheon, "Hybrid nanoparticles for magnetic resonance imaging of target-specific viral gene delivery," *Advanced Materials,* vol. 19, pp. 3109-3112, 2007.

[9] A. Jordan, R. Scholz, P. Wust, H. Fähling, and F. Roland, "Magnetic fluid hyperthermia (MFH): Cancer treatment with AC magnetic field induced excitation of biocompatible superparamagnetic nanoparticles," *Journal of Magnetism and Magnetic Materials,* vol. 201, pp. 413-419, 1999.

[10] A. Jordan, R. Scholz, P. Wust, H. Schirra, S. Thomas, H. Schmidt, and R. Felix, "Endocytosis of dextran and silan-coated magnetite nanoparticles and the effect of intracellular hyperthermia on human mammary carcinoma cells in vitro," *Journal of Magnetism and Magnetic Materials,* vol. 194, pp. 185-196, 1999.

[11] ""Hyperthermia in Cancer Treatment: Questions and Answers", [Online]. Available: http://www.cancer.gov/cancertopics/factsheet/Therapy/hyperthermia.."

[12] S. Laurent, D. Forge, M. Port, A. Roch, C. Robic, L. Vander Elst, and R. N. Muller, "Magnetic iron oxide nanoparticles: Synthesis, stabilization, vectorization, physicochemical characterizations and biological applications," *Chemical Reviews,* vol. 108, pp. 2064-2110, 2008.

[13] J. Giri and D. Bahadur, "Biomaterials and magnetism," *Sadhana - Academy Proceedings in Engineering Sciences,* vol. 28, pp. 639-656, 2003.

[14] A. Jordan, R. Scholz, P. Wust, H. Fähling, and F. Roland, "Magnetic fluid hyperthermia (MFH): Cancer treatment with AC magnetic field induced excitation of biocompatible superparamagnetic nanoparticles," *Journal of Magnetism and Magnetic Materials*, vol. 201, pp. 413-419, 1999.

[15] C. v. Blitterswijk, P. Thomsen, A. Lindahl, J. Hubbell, D. F. Williams, R. Cancedda, J. D. d. Bruijn, and J. Sohier, *Tissue Engineering*: Academic Press, 2008.

[16] ""Dorland's Medical Dictionary for Healthcare Consumers: Biocompatibility", [Online]. Available: http://www.mercksource.com/pp/us/cns/cns_hl_dorlands_split.jsp?pg=/ppdocs/us/common/dorlands/dorland/one/000012724.htm."

[17] A. K. Gupta and M. Gupta, "Synthesis and surface engineering of iron oxide nanoparticles for biomedical applications," *Biomaterials*, vol. 26, pp. 3995-4021, 2005.

[18] S. Laurent, D. Forge, M. Port, A. Roch, C. Robic, L. Vander Elst, and R. N. Muller, "Magnetic iron oxide nanoparticles: Synthesis, stabilization, vectorization, physicochemical characterizations and biological applications," *Chemical Reviews*, vol. 108, pp. 2064-2110, 2008.

[19] M. Ming, Z. Yu, Y. Wei, S. Hao-ying, Z. Hai-qian, and G. Ning, "Preparation and characterization of magnetite nanoparticles coated by amino silane," *Colloids and Surfaces A (Physicochemical and Engineering Aspects)*, vol. 212, pp. 219-26, 2003.

[20] S. Meerod, G. Tumcharern, U. Wichai, and M. Rutnakornpituk, "Magnetite nanoparticles stabilized with polymeric bilayer of poly(ethylene glycol) methyl ether-poly(ε-caprolactone) copolymers," *Polymer*, vol. 49, pp. 3950-3956, 2008.

[21] D. H. Kim, S. H. Lee, K. H. Im, K. N. Kim, K. M. Kim, I. B. Shim, M. H. Lee, and Y. K. Lee, "Surface-modified magnetite nanoparticles for hyperthermia: Preparation, characterization, and cytotoxicity studies," *Current Applied Physics*, vol. 6, pp. 242-246, 2006.

[22] L. M. Lacava, Z. G. M. Lacava, M. F. Da Silva, O. Silva, S. B. Chaves, R. B. Azevedo, F. Pelegrini, C. Gansau, N. Buske, D. Sabolovic, and P. C. Morais, "Magnetic resonance of a dextran-coated magnetic fluid intravenously administered in mice," *Biophysical Journal*, vol. 80, pp. 2483-6, 2001.

[23] P. Pradhan, J. Giri, R. Banerjee, J. Bellare, and D. Bahadur, "Cellular interactions of lauric acid and dextran-coated magnetite nanoparticles," *Journal of Magnetism and Magnetic Materials*, vol. 311, pp. 282-287, 2007.

[24] M. Lattuada and T. Alan Hatton, "Functionalized monodisperse magnetic nanoparticles," Cincinnati, OH, United States, 2005, p. 3042.

[25] T. K. Jain, J. Richey, M. Strand, D. L. Leslie-Pelecky, C. A. Flask, and V. Labhasetwar, "Magnetic nanoparticles with dual functional properties: Drug delivery and magnetic resonance imaging," *Biomaterials*, vol. 29, pp. 4012-4021, 2008.

[26] ""Ferumoxides (Systemic)", [Online]. Available: http://www.drugs.com/mmx/feridex-i-v.html#citec00702915."

[27] X. Q. Xu, H. Shen, J. R. Xu, J. Xu, X. J. Li, and X. M. Xiong, "Core-shell structure and magnetic properties of magnetite magnetic fluids stabilized with dextran," *Applied Surface Science,* vol. 252, pp. 494-500, 2005.

[28] T. H. T. Kawaguchi, M. Hasegawa, S. Maruno, "Dextran-magnetite complex: conformation of dextran chains and stability of solution," *Journal of Material Science: Materials in Medicine,* vol. 12, pp. 121-127, 2001.

[29] A. P. Herrera, C. Barrera, and C. Rinaldi, "Synthesis and functionalization of magnetite nanoparticles with aminopropyl-silane and carboxymethyl-dextran," *Journal of Materials Chemistry,* vol. 18, pp. 3650-3654, 2008.

[30] C. C. Berry, S. Wells, S. Charles, and A. S. G. Curtis, "Dextran and albumin derivatised iron oxide nanoparticles: Influence on fibroblasts in vitro," *Biomaterials,* vol. 24, pp. 4551-4557, 2003.

[31] J. Clement, M. Schwalbe, N. Buske, K. Wagner, M. Schnabelrauch, P. Görnert, K. Kliche, K. Pachmann, W. Weitschies, and K. Höffken, "Differential interaction of magnetic nanoparticles with tumor cells and peripheral blood cells," *Journal of Cancer Research and Clinical Oncology,* vol. 132, pp. 287-292, 2006.

[32] S. W. C.C. Berry, S. Charles, A.S.G. Curtis "Dextran and albumin derivatised iron oxide nanoparticles: influence on fibroblasts in vitro," *Biomaterials,* vol. 24, pp. 4551-4557, 2003.

[33] U. Gaur, S. K. Sahoo, T. K. De, P. C. Ghosh, A. Maitra, and P. K. Ghosh, "Biodistribution of fluoresceinated dextran using novel nanoparticles evading reticuloendothelial system," *International Journal of Pharmaceutics,* vol. 202, pp. 1-10, 2000.

[34] M. S. J.H. Clement, N. Buske, K. Wagner, M. Schnabelrauch, P. Görnert, K.K. Kliche, K. Pachmann, W. Weitschies, K. Höffken, "Differential interation of magnetic nanoparticles with tumor cells and peripheral blood cells," *J Cancer Res Clin Oncol,* vol. 132, pp. 287-292, 2006.

[35] Y. Zhang and J. Zhang, "Surface modification of monodisperse magnetite nanoparticles for improved intracellular uptake to breast cancer cells," *Journal of Colloid and Interface Science,* vol. 283, pp. 352-357, 2005.

[36] S. W. C.C. Berry, S. Charles, G. Aitchison, A.S.G. Curtis, "Cell response to dextran-derivatised iron oxide nanoparticles post internalization," *Biomaterials,* vol. 25, pp. 5405-5413, 2004.

[37] C. B. C. Wilhelm, J. Roger, J.N. Pons, J.-C. Bacri, F. Gazeau, "Intracellular uptake of anionic superparamagnetic nanoparticles as a function of their surface coating," *Biomaterials,* vol. 24, pp. 1001-1011, 2003.

[38] D. L. J. Thorek and A. Tsourkas, "Size, charge and concentration dependent uptake of iron oxide particles by non-phagocytic cells," *Biomaterials,* vol. 29, pp. 3583-90, 2008.

[39] M. R. Lorenz, V. Holzapfel, A. Musyanovych, K. Nothelfer, P. Walther, H. Frank, K. Landfester, H. Schrezenmeier, and V. Mailander, "Uptake of functionalized, fluorescent-labeled polymeric particles in different cell lines and stem cells," *Biomaterials,* vol. 27, pp. 2820-2828, 2006.

[40] A. Ito, M. Shinkai, H. Honda, and T. Kobayashi, "Medical application of functionalized magnetic nanoparticles," *Journal of Bioscience and Bioengineering,* vol. 100, pp. 1-11, 2005.

[41] F. C. R. Huynh, J. Jozefonvicz, "Carboxymethylation of dextran in aqueous alcohol as the first step of the preparation of derivatized dextrans," *Die Angewandte Makromolekulare Chemie*, vol. 254, pp. 61-65, 1998.

[42] J. C. F. Chaubet, O. Maïga, S. Mauray, J. Jozefonvicz, "Synthesis and structure-anticoagulant property relationships of functionalized dextrans: CMDBS," *Carbohydrate Polymers*, vol. 28, pp. 145-152, 1995.

[43] E. D. K. R.W. Eyler, F. Diephuis, "Determination of degree of substitution of sodium carboxymethylcellulose," *Analytical Chemistry*, vol. 19, 1947.

[44] K. Park, Y. Hwang, J. Park, H. Noh, J. Kim, N. Hwang, and T. Hyeon, "Ultra large-scale synthesis of monodisperse nanocrystals," *Nature*, vol. 3, pp. 891-895, 2004.

[45] R. De Palma, S. Peeters, M. Van Bael, H. Van den Rul, K. Bonroy, W. Laureyn, J. Mullens, G. Borghs, and G. Maes, "Silane ligand exchange to make hydrophobic superparamagnetic nanoparticles water-dispersible.," *Chemistry of Materials*, vol. 19, pp. 1821-1831, 2007.

[46] D. Lin-Vien, N. B. Colthup, W. G. Fateley, and J. G. Grasselli, *The Handbook of Infrared and Raman Characteristic Frequencies of Organic Molecules*. San Diego, California: Academic Press, 1991.

[47] M. De, P.S. Chosh, and V.M. Rotello, "Applications of Nanoparticles in Biology," *Advanced Materials*, vol. 20, pp. 1-17, 2008.

[48] J. Panyam, and V. Labhasetwar, " Biodegradable nanoparticles for drug and gene delivery to cells and tissues", *Advanced Drug Delivery Reviews*, vol. 55, pp.329-347, 2003.

[49] I. Bremner, J.S.G. Cox, and G. F. Moss, " Structural Studies on Iron-Dextran" *Carbohydrate Research*,vol. 11, pp. 77-84, 1969.

[50] A. Engel, Michael F. Frey, C. Jeffrey Lacey, and Roger A. Egolf, " Carboxymethyl dextran lactone: A preactivated polymer for amine conjugations", *Bioconjugate Chem.*, vol. 5, pp. 98-100, 1994.

APPENDIX A

Summary of the variation in carboxymethylation reaction parameters and obtained results

Sample #	[NaOH]	[MCA]/[Dextran]	T (ºC)	Reaction steps	Solvent	Reaction time (min)	DS	COOH/chain
1	1M	2.5	60	1	Water	75	0.03	1.70-1.96
2	2M	2.5	60	1	50:50 Water/ Isopropanol	75	0.04-0.05	3.93-4.59
3	2M	0.4	60	1	Water	75	.04	3.67
4	2M	2.5	60	1	Water	75	0.07-0.08	4.24-4.97
5	2M	2.5	60	1	Water	30	0.08	4.78
6	2M	2.5	60	1	Water	45	0.09	5.28
7	2M	24	60	1	Water	75	0.08	7.05
8	2M	0.02	50	1	Water	75	0.7	6.98
9	3M	2.5	60	1	Water	75	0.38	23.40
10	3M	2.5	60	2	Water	75	0.61	38.00

APPENDIX B

Hydrodynamic diameter (Dh) distributions from DLS measurement

Hydrodynamic diameter results shown in chapter 4 were the diameter corresponding to a number relative intensity of 100. However for a same sample measurement a range of diameters with different intensities are obtained. Here we shown the obtained size distribution for each DLS measurement.

B.1 Size distribution of Magnetite-APS-CMDx 5 samples for the pH studied range.

Sample 1

pH= 10. 0

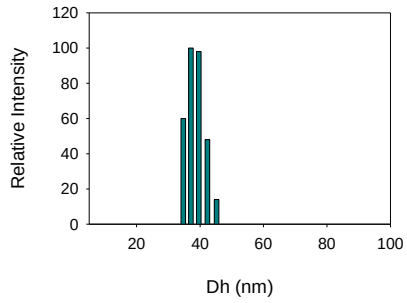

Sample 2

pH= 10. 0

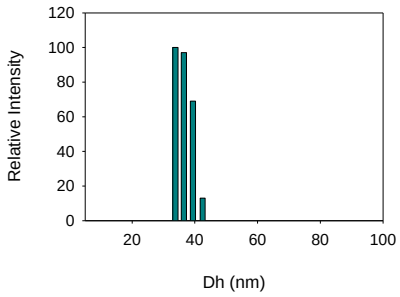

pH= 8.0

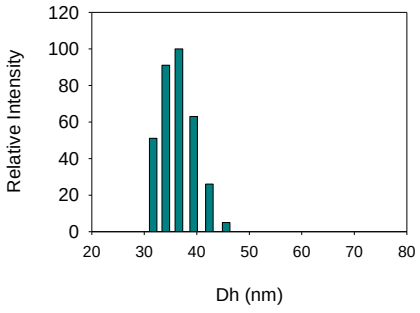

pH= 8.0

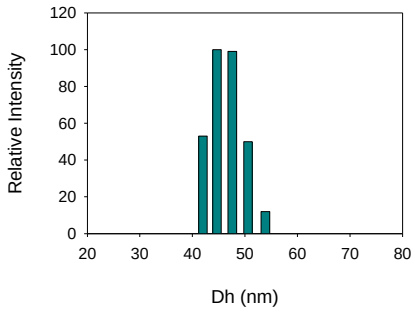

Sample 1

Sample 2

pH= 7.0

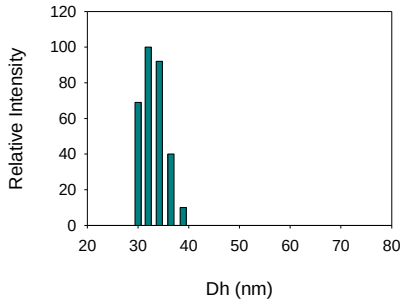

pH= 7.0

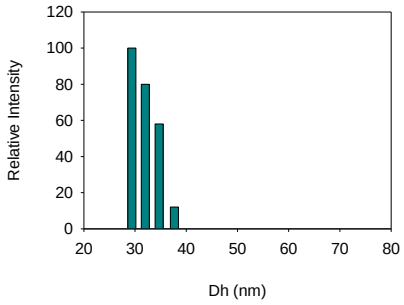

pH= 5.0

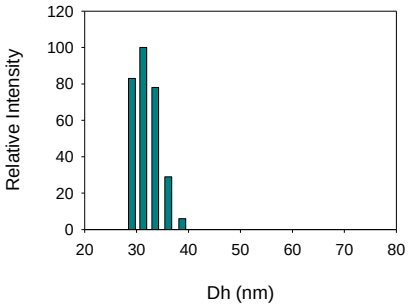

pH= 5.0

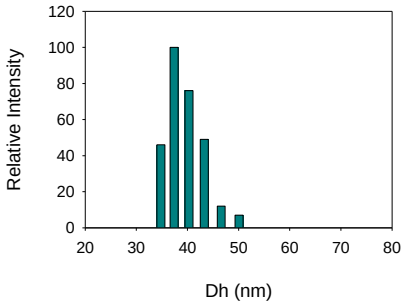

pH= 2.0

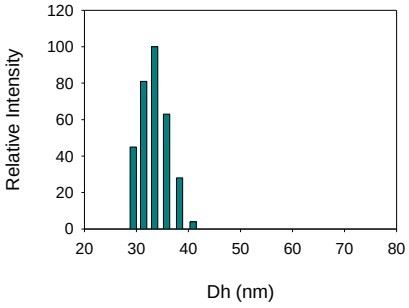

pH= 2.0

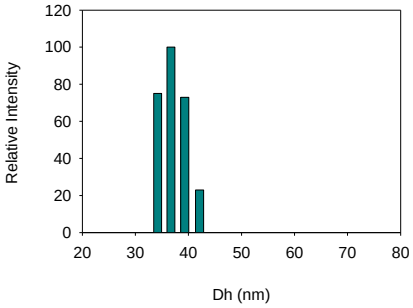

B.2 Size distribution for Magnetite-APS-CMDx 23 samples for the pH range studied.

Sample 1

pH= 10. 0

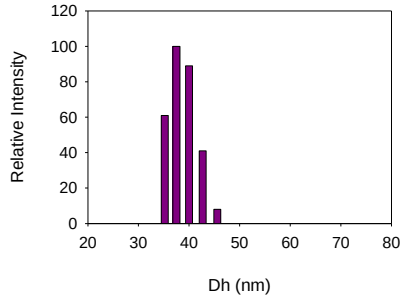

pH= 8.0

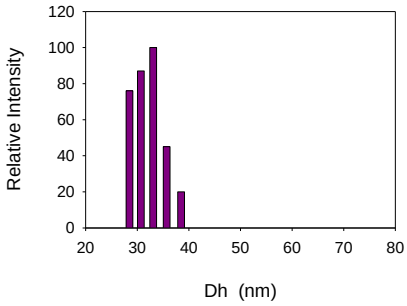

pH= 7.0

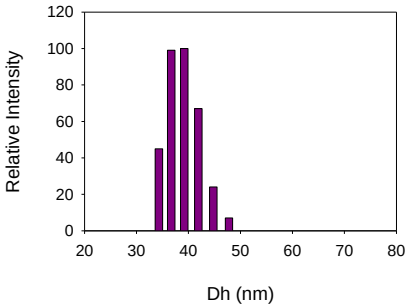

Sample 2

pH= 10. 0

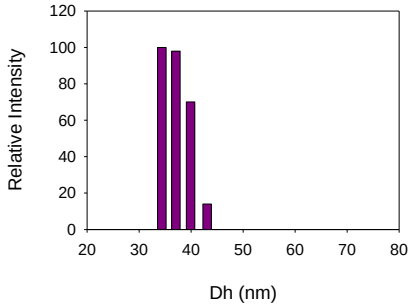

pH= 8.0

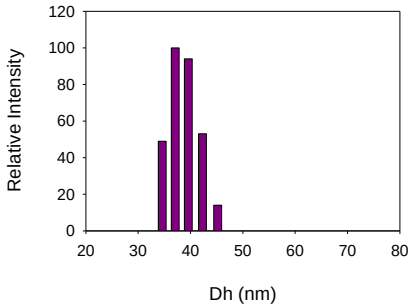

pH= 7.0

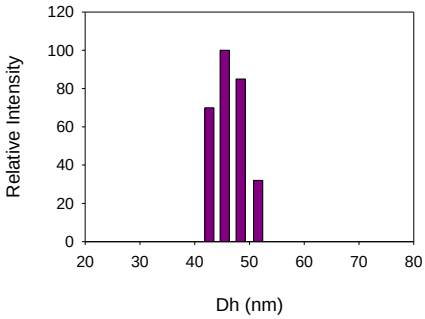

Sample 1
pH= 5.0

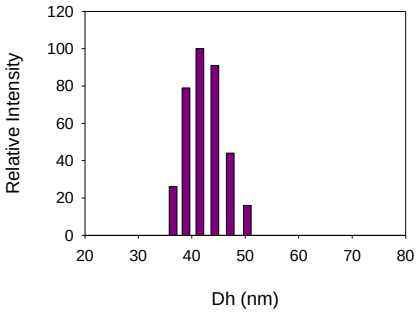

Sample 2
pH= 5.0

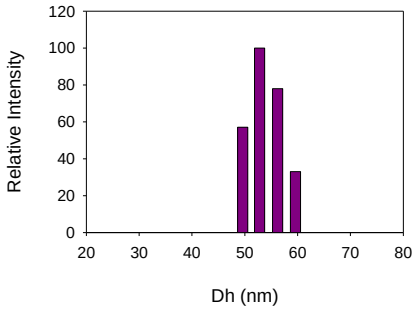

pH= 2.0

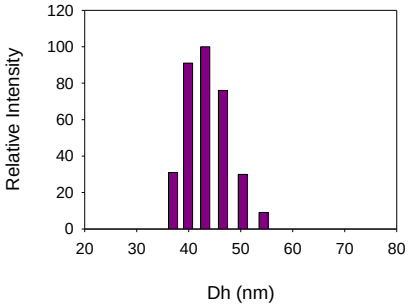

pH= 2.0

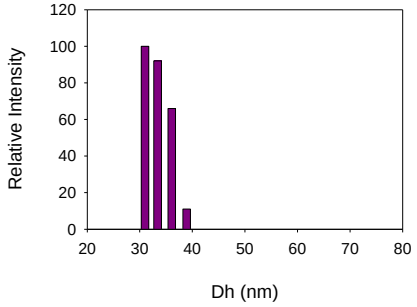

B.3 Size distribution for Magnetite-APS-CMDx 38 samples for the pH range studied.

Sample 1

pH= 10. 0

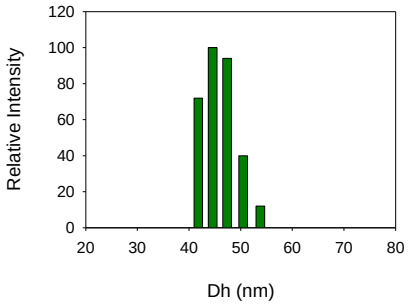

Sample 2

pH= 10. 0

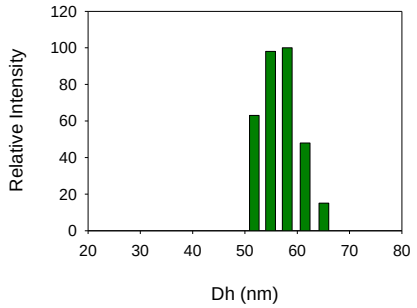

Sample 1
pH= 8.0

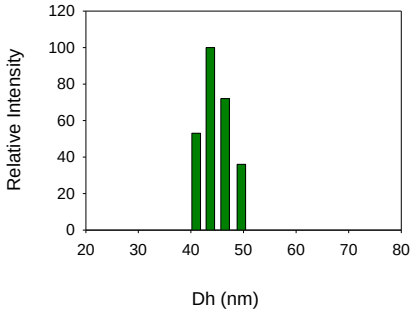

Sample 2
pH= 8.0

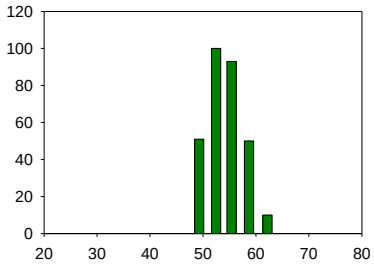

pH= 7.0

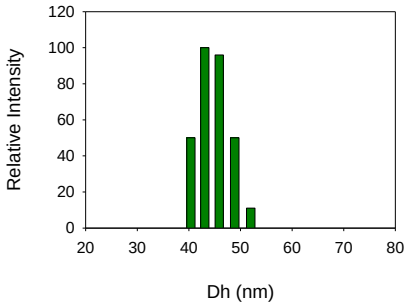

pH= 7.0

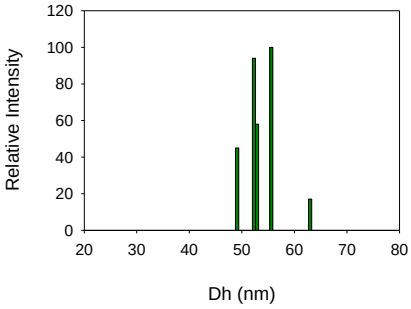

pH= 5.0

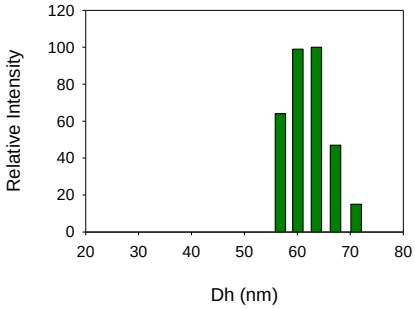

pH= 5.0

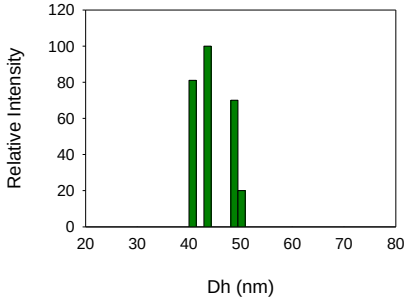

Sample 1
pH= 2.0

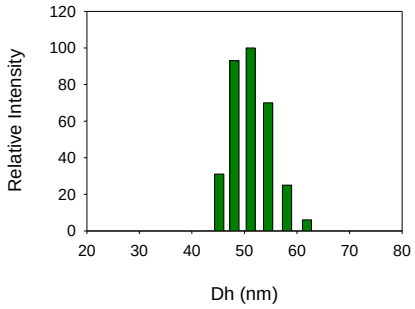

Sample 2
pH= 2.0

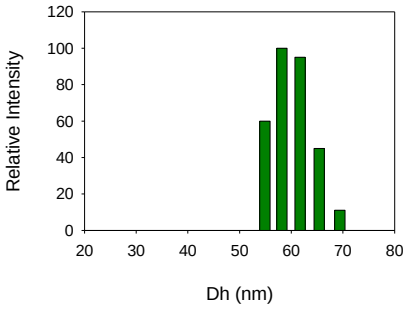

B.4 Size distribution for Magnetite-APS-CMDx 5 samples for the NaCl concentrations studied.

Sample 1

[NaCl]= 0.0190 M

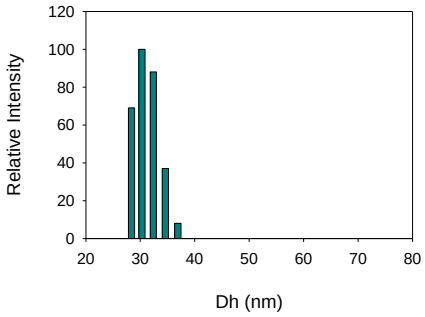

Sample 2

[NaCl]= 0.0190 M

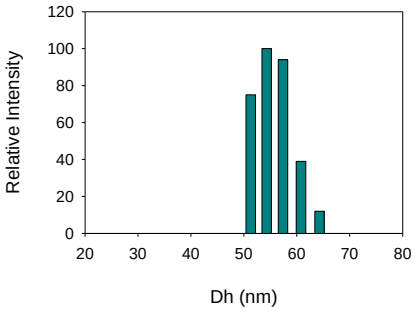

[NaCl] = 0.0345 M

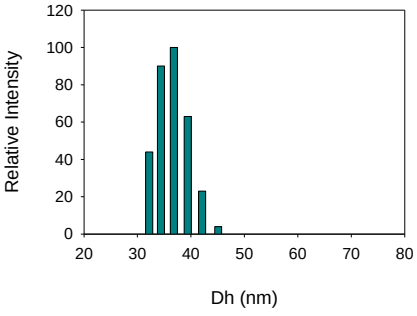

[NaCl] = 0.0345 M

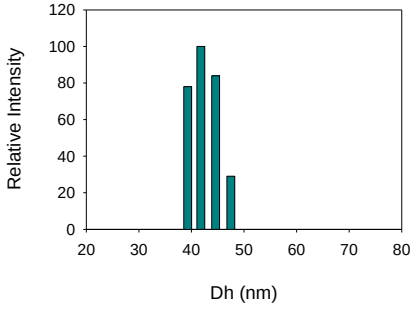

Sample 1
[NaCl]= 0.0690 M

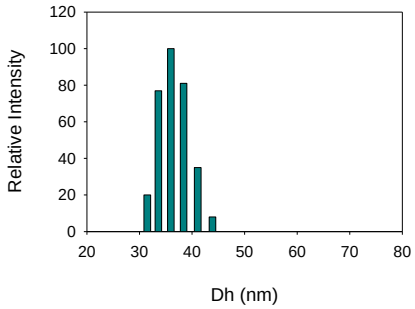

Sample 2
[NaCl]= 0.0690 M

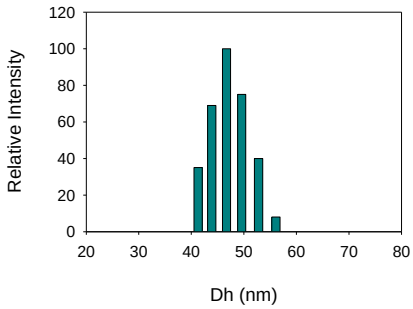

[NaCl]= 0.1380 M

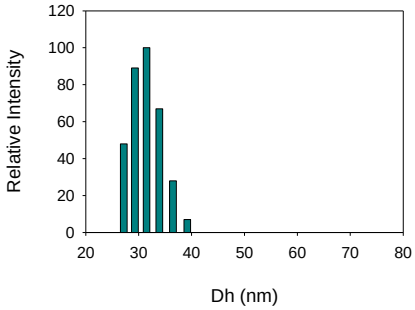

[NaCl]= 0.1380 M

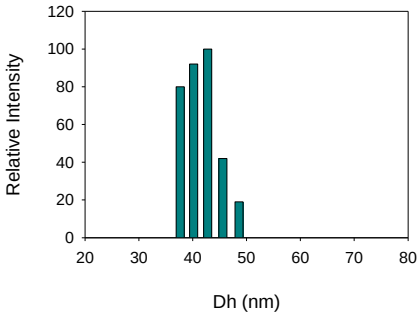

B.5 Size distribution for Magnetite-APS-CMDx 23 samples for the NaCl concentrations studied.

Sample 1

[NaCl]= 0.0190 M

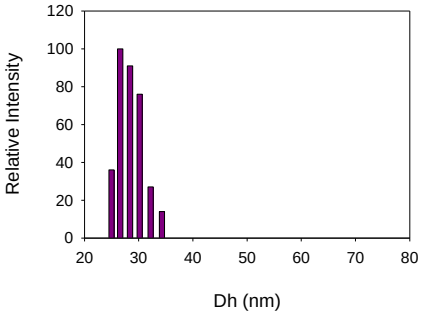

Sample 2

[NaCl]= 0.0190 M

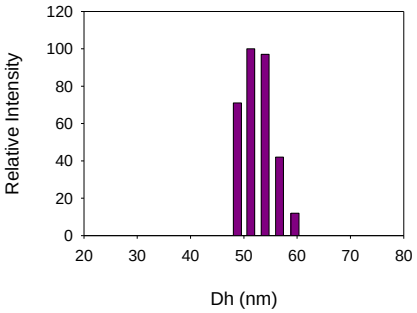

Sample 1
[NaCl] = 0.0345 M

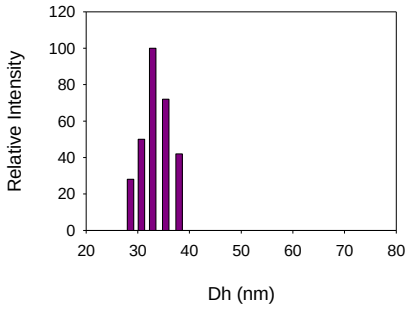

[NaCl]= 0.0690 M

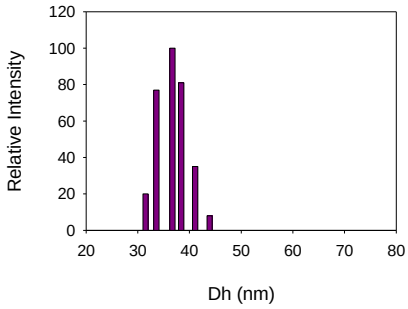

[NaCl]= 0.1380 M

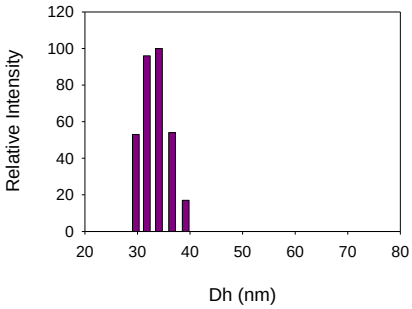

Sample 2
[NaCl] = 0.0345 M

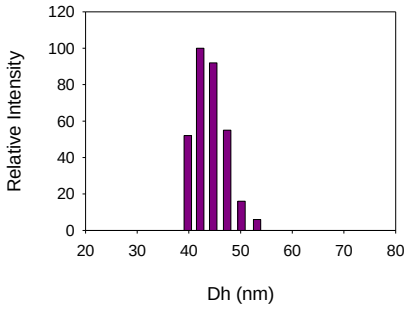

[NaCl]= 0.0690 M

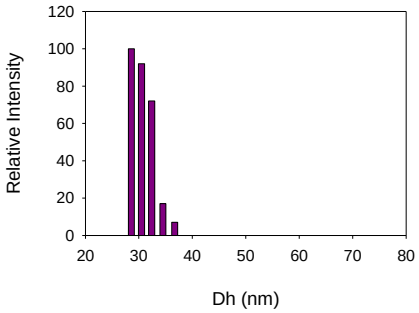

[NaCl]= 0.1380 M

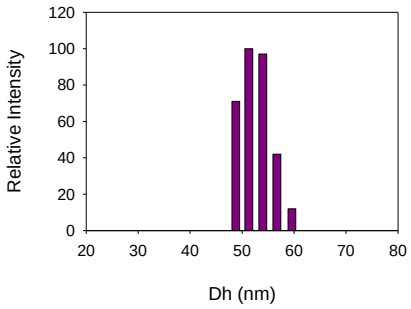

B.6 Size distribution for Magnetite-APS-CMDx 38 samples for the NaCl concentrations studied.

Sample 1

[NaCl]= 0.0190 M

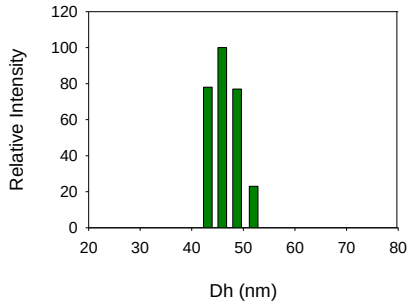

Sample 2

[NaCl]= 0.0190 M

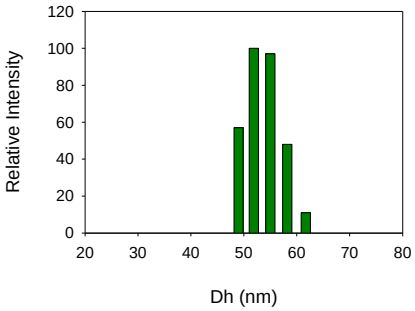

[NaCl] = 0.0345 M

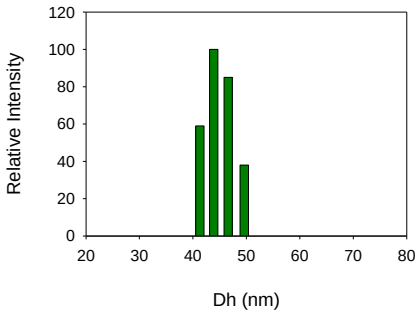

[NaCl] = 0.0345 M

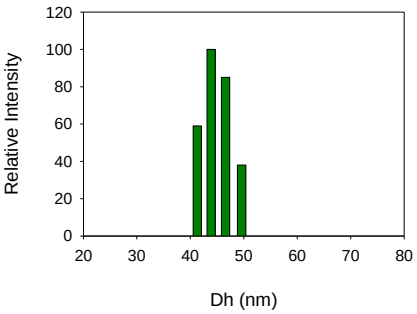

[NaCl]= 0.0690 M

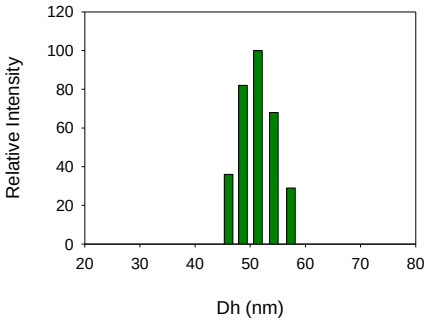

[NaCl]= 0.0690 M

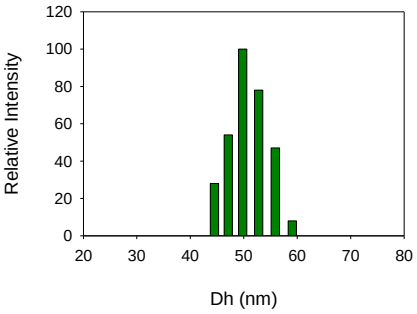

Sample 1
[NaCl]= 0.1380 M

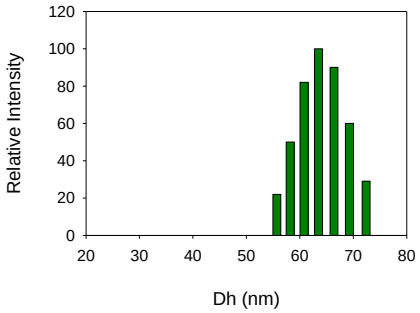

Sample 2
[NaCl]= 0.1380 M